

1 **Characteristics of aerosol pollution during heavy haze events**
2 **in Suzhou, China**

3

4 **M. Tian¹, H. B. Wang¹, Y. Chen¹, F. M. Yang^{1,2,3*}, X. H. zhang^{4,2}, Q. Zou^{4,2}, R. Q.**
5 **Zhang^{4,2}, Y. L. Ma^{5,3}, K. B. He^{5,3}**

6 ¹Key Laboratory of Reservoir Aquatic Environment of CAS, Chongqing Institute of
7 Green and Intelligent Technology, Chinese Academy of Sciences, Chongqing 400714,
8 China

9 ²Center for Excellence in Urban Atmospheric Environment, Institute of Urban
10 Environment, Chinese Academy of Sciences, Xiamen 361021, China

11 ³Changjiang Normal University, Chongqing 408100, China.

12 ⁴Suzhou Environmental Monitoring Center, Suzhou 215004, China

13 ^{3,5}School of Environment, Tsinghua University, Beijing 100012, China

14 *Correspondence to:* F. M. Yang (fmyang@cigit.ac.cn)

15

16 **Abstract**

17 ~~A comprehensive measurement was carried out to analyze the heavy haze events in~~
18 ~~Suzhou in January 2013 when extremely severe haze weather events~~~~pollution~~
19 occurred in many cities in China, especially in the ~~East part of the country, in~~
20 ~~January 2013. Comprehensive measurements including hourly concentrations of~~
21 ~~PM_{2.5}, and its major chemical components~~~~sition~~ (including water-soluble inorganic
22 ions, OC, and EC), and ~~related~~ gas-phase precursors were ~~obtained~~~~conducted~~ via
23 on-line monitoring system ~~in Suzhou, a medium size city of Jiangsu province, just~~
24 ~~east of Shanghai. Based on these data, detailed aerosol composition, light extinction~~
25 ~~and gas-phase precursors were analyzed to understand the characteristics of the haze~~
26 ~~events, moreover, the formation mechanism of nitrate and sulfate in PM_{2.5} and the~~
27 ~~regional sources deduced from trajectory and PSCF were discussed to explore the~~
28 ~~origin of the heavy aerosol pollution. The results showed that frequent haze events~~
29 ~~were occurred on Jan. 2013 and the concentrations of PM_{2.5} frequently~~~~often~~
30 ~~exceeded 150 μg m⁻³ on hazy days during the haze occurrence, with the~~ maximum
31 ~~reaching concentration of 324 μg m⁻³ on Jan. 14, 2013. Unfavorable weather~~
32 conditions (high RH, and low rainfall, wind speed and atmospheric pressure) ~~were~~
33 ~~conducive for the haze formation. High concentrations~~ of secondary aerosol species
34 (including SO₄²⁻, NO₃⁻, NH₄⁺, and SOC) and ~~gaseous~~ precursors were observed during
35 the ~~first two~~ haze events, ~~while elevated primary carbonaceous species emissions~~
36 ~~were found during the third haze period, pointing to different haze formation~~
37 ~~mechanisms. Additionally, OM, (NH₄)₂SO₄, NH₄NO₃ were demonstrated~~~~found~~ to be
38 the major contributors to ~~the~~ visibility impairment ~~but the share differed from haze~~
39 ~~events. This study also found that the high concentrations~~ of sulfate ~~and nitrate~~
40 might be explained by ~~the~~ ~~homogeneous gas-phase reactions under low RH conditions~~
41 ~~and by heterogeneous processes under relatively high RH conditions. heterogeneous~~
42 ~~reactions in the aqueous surface layer of pre-existing particles or in cloud processes~~
43 ~~while nitrate might be mainly formed through homogeneous gas-phase reactions. The~~
44 ~~results of Analysis of air mass trajectory clustering and potential source contribution~~
45 ~~function~~~~the PSCF method~~ manifested that aerosol pollutions in the studied areas were

46 mainly ~~caused~~~~affected~~ by local activities and surrounding sources transported from
47 nearby cities.

48

49 1. Introduction

50 ~~High occurrence of haze events (is defined as~~ visibility lower than 10 km
51 ~~when under the conditions of~~ relative humidity < 80%.) Rapidly increased air
52 pollution in China in the past several decades have resulted in frequent occurrences of
53 haze events, which have caused~~is of~~ great concern to the scientific community as well
54 ~~as both scientists and the public (Zhang et al., 2012). in China in recent years because~~
55 ~~of its~~ Haze events have great adverse effects on ~~the people's~~human health, traffic,
56 climate, and other important aspects (Zhang et al., 2015; Charlson et al., 1987;
57 Ramanathan and Vogelmann, 1997; Tegen et al., 2000; Yu et al., 2002; Tie et al.,
58 2009a; Tie et al., 2009b). Fine particles (PM_{2.5}, aerosols with an aerodynamic
59 diameter of 2.5 microns or less) ~~are~~has a largely responsible for haze formation due to
60 their ability in impact on visibility by light extinction including scattering and
61 absorbing solar and infrared radiation ~~and is mainly responsible for the formation of~~
62 ~~haze~~(Yu et al., 2014). ~~The~~Light extinction of PM_{2.5} is highly associated with ~~its~~the
63 chemical compositions (Tao et al., 2014). Water-soluble inorganic ions and
64 carbonaceous species often account for major fractions of PM_{2.5} and are important
65 contributors to visibility impairment (Tan et al., 2009; Pathak et al., 2009), and thus
66 have been. ~~Therefore, these species were emphatically~~ investigated extensively in
67 researches related to haze occurrence (Yang et al., 2005; Jansen et al., 2014; Pathak et
68 al., 2009). ~~However, most of these existing~~ studies were based on ~~artificial filter~~
69 sampling and off-line analysis ~~and had~~which has its limitations ~~of in~~ providing
70 detailed insight into the roles ~~of the major chemical~~these species played during shorter
71 haze periods.

72 High contributions of secondary inorganic aerosols (SIA, including sulfate,
73 nitrate and ammonium), the predominant water-soluble ionic species in PM_{2.5}, to
74 visibility reduction have been observed in many cities in China (Huang et al., 2014).

75 Gas-phase or liquid-phase reactions of sulfur dioxide and nitrogen oxides ~~are~~ the
76 primary ~~mechanisms forming source of~~ aerosol sulfate and nitrate. For the formation
77 of sulfate, homogeneous gas phase reaction of SO₂ with OH radical, ~~and~~
78 heterogeneous reactions in the aqueous surface layer of pre-existing particles, and
79 in-cloud processes are the primary mechanisms (Wang et al., 2006). The rates of
80 gas-phase and liquid-phase reactions of SO₂ were ~~close~~ similar in summer while the
81 heterogeneous processes were responsible for the oxidation in winter (Hewitt, 2001).
82 Nitric acid can be formed from homogeneous gas-phase reactions of NO₂ with OH or
83 O₃ and from heterogeneous hydrolysis of N₂O₅, which occurred predominantly during
84 daytime and nighttime, respectively (Khoder, 2002). Both sulfuric acid and nitric acid
85 ~~will~~ react with alkaline substance in the atmosphere, mostly ammonia under ambient
86 conditions to produce salts (Hewitt, 2001). The neutralization of sulfuric acid by
87 ammonia has been found to be preferred over the formation of ammonium nitrate
88 (Warneck, 1999). Thus, the formation of ammonium nitrate in fine particles is usually
89 under significantly neutralized or ammonium-rich ~~sulfate~~ conditions (Pathak et al.,
90 2009). There are various factors influencing the formation of aerosol sulfate and
91 nitrate, such as the levels of gaseous precursors (SO₂, NH₃, NO_x) and oxidants, the
92 characteristics of pre-existing aerosols, and meteorological conditions. These factors
93 may vary by location, ~~this may~~ resulting in different formation mechanism in different
94 areas. For instance, different formation pathways had been reported for nitrate in
95 ammonia-rich and ammonia-deficient areas (Pathak et al., 2009).

96 ~~Due to the rapid economic and industrial developments and urbanization in past~~
97 ~~few decades, the visibility reduction become increasingly serious in China, especially~~
98 ~~in the East (Zhang et al., 2012).~~ In January 2013, extremely severe, persistent and
99 widespread haze weather occurred in 10 provinces, ~~regions and cities~~ in central and
100 eastern China. These serious pollution events not only ~~had~~ great adverse effects on
101 human health, ~~as seen in~~ caused a sharp increase in respiratory diseases, but also
102 caused immeasurable economic loss (Huang et al., 2014; Chen et al., 2013). High
103 secondary inorganic and organic aerosol contributions to particulate pollution during

104 these haze events were reported in a recent study based on the measurements at urban
105 sites in Beijing, Shanghai, Guangzhou and Xi'an, which located in the northern,
106 eastern, southern and western regions of China, respectively (Huang et al., 2014).

107 ~~This result indicated that i~~In addition to ~~investigating~~investigate the primary particulate
108 emissions, ~~it's also important to explore~~the formation mechanisms ~~and effect factors~~
109 of these secondary species and related affecting factors also need to be understood in
110 order to controlling PM_{2.5} levels in China.

111 The Yangtze River Delta (YRD), ~~together with~~the Pearl River Delta,
112 Beijing-Tianjin-Tangshan, and the Sichuan Basin are ~~of most interesting as they are~~
113 the four regions with heaviest haze ~~influence~~regions in China. The characteristics and
114 formation mechanisms of haze in the YRD are different from other haze regions, such
115 as Beijing and the Pearl River Delta (Fu et al., 2008). Suzhou is located in the
116 heartland of YRD region and is an important city ~~in the YRD~~. ~~Suzhou~~It suffered from
117 the extremely serious aerosol pollution in Jan. 2013. With the tremendous economic
118 growth over the past 30 years, Suzhou has experienceds high levels of air pollution as
119 reflected in the frequency of haze occurrence. The annually haze days in Suzhou
120 increased from only two days to more than 150 days from 1956 to 2011, i.e. over 40%
121 of days were hazy in 2011. The lower visibility, particularly the haze, has become a
122 major concern of the citys. ~~h~~However, only a few ~~studies~~researches have focused
123 ~~on been carried out to study the~~ haze events in Suzhou and. ~~L~~Little is known about the
124 chemical characteristics and sources of fine particles in this city~~Suzhou~~. To fill these
125 knowledge gaps~~Therefore~~, an intensified monitoring campaign was launched from
126 December 2012 to January 2013 to ~~collect~~get insight into the haze occurrence in
127 ~~urban Suzhou~~. ~~On the basis of~~ high temporal resolution chemical and ~~measurements~~
128 ~~combined with~~ meteorological datas. ~~t~~The objectives of this study are to (1) identify
129 the dominant species in PM_{2.5} and responsible for the visibility reduction; (2) explore
130 the formation mechanism of the aerosol pollution; (3) study the impact of local,
131 nearby and ~~remote~~transport sources on the formation of haze in urban Suzhou.

132

133 2. Methodology

134 2.1 Field observations

135 The sampling station was set up at the roof of ~~one~~the building in Suzhou Institute of
136 Environmental Sciences (31°20'N, 120°36'E) (Fig. 1), about 300 m west to Nanyuan
137 South Road and 360 m north to S Ring Road Elevated Bridge. There is no industrial
138 source nearby and ~~the~~is site is representative of an urban residential and commercial
139 ~~environment~~-area. Suzhou is located in the center of Yangtze River Delta (YRD) and
140 about 80 km east ~~of~~ Shanghai and 200 km west ~~of~~ Nanjing.

141 ~~On-line hourly PM_{2.5} mass concentrations, ionic species and OC/EC were~~
142 ~~measured by tapered element oscillating microbalance (TOEM), URG 9000 Ion~~
143 ~~Chromatography, Sunset semi-continuous OC/EC analyzer, respectively. On-line~~
144 hourly PM_{2.5} mass concentrations were measured using tapered element oscillating
145 microbalance (TEOM1405, Thermo Scientific Corp., MA, US) with the heating
146 temperature of 50 °C. Some of the volatile particulate matter might be lost at 50 °C,
147 but comparisons with collocated filters showed that the loss was less than 10%-20%
148 of the gravimetric mass (Chow et al., 2008).

149 Hourly real-time concentrations of five cations (Na⁺, K⁺, NH₄⁺, Ca²⁺, and Mg²⁺)
150 and four anions (F⁻, Cl⁻, NO₃⁻, and SO₄²⁻) in PM_{2.5} were determined by URG Series
151 9000 Ambient Ion Monitor (AIM, URG Corporation, Chapel Hill, NC). The system
152 consists of a particle collection unit and two ion chromatograph analyzers for cation
153 and anion analyses. PM_{2.5} was separated by a sharp-cut cyclone inlet operating at a
154 flow rate of 3 L/min. The air was drawn through a liquid diffusion parallel-plate
155 denuder to remove the interfering acidic and basic gases. A Steam-Jet Aerosol
156 Collector was placed downstream of the denuder for collection and extraction of
157 particles. The water extract was subsequently injected into the two ICs once an hour.
158 The estimated uncertainties of the AIM measurements were approximately less than
159 15% (Trebs et al., 2004; Pathak et al., 2011). Some measures were taken out to reduce
160 error, for instance, standards solutions were periodically injected to check the

161 consistency of sensitivity of the detectors and air flow rate is frequently checked using
162 a calibrated flow meter.

163 A semi-continuous OC/EC analyzer (Sunset Laboratory, Forest Grove, Oregon,
164 USA) was applied to determine the carbonaceous species in PM_{2.5}. This instrument
165 used the thermal-optical transmittance method based on NIOSH Method 5040.
166 Organic compounds were vaporized in pure helium and then oxidized to CO₂ in a
167 manganese dioxide oxidizing oven. CO₂ was then quantified by non-dispersive
168 infrared detector. EC was then desorbed in an oxygen blend carrier gas and then
169 oxidized and quantified using the same method as for OC. The split point between the
170 pyrolyzed carbon formed from the organic carbon during the heating and EC that was
171 originally in the sample was determined by measuring the transmission of a laser
172 beam through the filter. Known volume of methane was injected, oxidized and
173 quantified as an internal standard. Good correlations were found between the data
174 measured by this instrument and filter-based laboratory analyses (Bae et al., 2004).

175 Visibility was monitored using the Belfort Model 6000 Visibility Sensor (Belfort
176 Instrument Corp., MD, US). Trace O₃, SO₂, NO-NO₂-NO_x and CO gases were
177 obtained with a resolution of 1 h by applying online analyzers (Thermo Instruments,
178 TEI 49i, 43i, 42i and 48i, respectively) (Wang, 2016 #343). Meteorological
179 parameters were collected using Met Station One (Met One Corp., OR, US).

181 **2.2 Data analysis methods**

182 **2.2.1 Reconstruction of the light extinction coefficient**

183 The light extinction (b_{ext}) which is the sum of light scattering by particle ($b_{\text{s,p}}$),
184 absorption by particle ($b_{\text{a,p}}$), scattering by gas ($b_{\text{s,g}}$), and absorption by gas ($b_{\text{a,g}}$), is
185 reconstructed according to the revised IMPROVE algorithm as following (Pitchford et
186 al., 2007):

$$187 \quad b_{\text{ext}} = b_{\text{s,p}} + b_{\text{a,p}} + b_{\text{a,g}} + b_{\text{s,g}}$$

$$\begin{aligned}
188 \quad & \approx 2.2 \times f_s(\text{RH}) \times [\text{Small } (\text{NH}_4)_2\text{SO}_4] + 4.8 \times f_L(\text{RH}) \times [\text{Large } (\text{NH}_4)_2\text{SO}_4] \\
189 \quad & + 2.4 \times f_s(\text{RH}) \times [\text{Small } \text{NH}_4\text{NO}_3] + 5.1 \times f_L(\text{RH}) \times [\text{Large } \text{NH}_4\text{NO}_3] \\
190 \quad & + 2.8 \times [\text{Small OM}] + 6.1 \times [\text{Large OM}] \\
191 \quad & + 1 \times [\text{Fine Soil}] + 1.7 \times f_{ss}(\text{RH}) \times [\text{Sea Salt}] \\
192 \quad & + 0.6 \times [\text{Coarse Mass}] + 10 \times [\text{EC Mass}] \\
193 \quad & + 0.33 \times [\text{NO}_2 \text{ (ppb)}] + \text{Rayleigh Scattering} \quad (1)
\end{aligned}$$

194 where $f_s(\text{RH})$ and $f_L(\text{RH})$ are the water growth factors for small- and large-sized
195 distribution of sulfate and nitrate, respectively; and $f_{ss}(\text{RH})$ is the water growth factor
196 for sea salt. Water growth factors are adopted according to Pitchford~~Isakov~~ et al.
197 (Pitchford et al., 2007)~~(Isakov et al., 2007)~~. The constant numbers in the above
198 equation are extinction efficiencies for each chemical species under dry condition.
199 $(\text{NH}_4)_2\text{SO}_4$ mass is estimated as 1.38 times of~~by the~~ SO_4^{2-} mass ~~multiplied by a factor~~
200 ~~of 1.38~~, and ~~the~~ NH_4NO_3 mass is estimated by the 1.29 times of NO_3^- mass ~~multiplied~~
201 ~~by a factor of 1.29 based on the assumption~~ that SO_4^{2-} and NO_3^- are fully
202 neutralized by NH_4^+ in the forms of $(\text{NH}_4)_2\text{SO}_4$ and NH_4NO_3 , respectively, according
203 to the revised IMPROVE method. Organic matter (OM) is estimated as 1.8 times
204 ~~of derived from multiplying~~ OC concentrations ~~by a factor of 1.8~~ to account for
205 unmeasured fractions~~atoms~~.

206 The concentrations of sulfate, nitrate, and OM are divided into small- and
207 large-sized fractions in this algorithm. The size modes are described by log-normal
208 mass size distributions with geometric mean diameter and geometric standard
209 deviations. Concentrations of sulfate, nitrate, and OM in the large- and small-mode
210 are estimated ~~by~~ using the following equations (taking sulfate as an example):

$$211 \quad [\text{Large } (\text{NH}_4)_2\text{SO}_4] = [\text{Total } (\text{NH}_4)_2\text{SO}_4]^2/20, \text{ for } [\text{Total } (\text{NH}_4)_2\text{SO}_4] < 20 \mu\text{g m}^{-3} \quad (2)$$

$$212 \quad [\text{Large } (\text{NH}_4)_2\text{SO}_4] = [\text{Total } (\text{NH}_4)_2\text{SO}_4], \text{ for } [\text{Total } (\text{NH}_4)_2\text{SO}_4] > 20 \mu\text{g m}^{-3} \quad (3)$$

$$213 \quad [\text{Small } (\text{NH}_4)_2\text{SO}_4] = [\text{Total } (\text{NH}_4)_2\text{SO}_4] - [\text{Large } (\text{NH}_4)_2\text{SO}_4] \quad (4)$$

214

215 **2.2.2 Air mass back trajectory**

216 To study the impact of local and regional sources on the aerosol pollution in Suzhou,
217 ~~the~~ 48-h back trajectories starting at 100 m from the sampling site were calculated ~~by~~
218 using the NOAA HYSPLIT model (http://ready.arl.noaa.gov/HYSPLIT_traj.php). The
219 back trajectories were calculated four times per day at starting times of 04:00, 10:00,
220 16:00, and 22:00 UTC, i.e. 12:00, 18:00, 00:00, and 06:00 local times, respectively.
221 The trajectory cluster analysis was based on the GIS-based software TrajStat (Wang et
222 al., 2009).

223

224 **2.2.3 Potential source contribution function**

225 The potential source contribution function (PSCF) method is based on the results of
226 HYSPLIT model and can be used to identify the regional sources. The zone of
227 concern is divided into $i \times j$ small equal grid cells. The PSCF value for the ij th grid
228 cell is calculated as: $PSCF_{ij} = m_{ij}/n_{ij}$, where n_{ij} is designated as the number of
229 trajectory segment endpoints that fall in the ij th cell and m_{ij} is defined as the number
230 of trajectory endpoints with pollutants concentrations higher than an set criterion
231 (Ashbaugh et al., 1985; Wang et al., 2009). In present study, the average
232 concentrations were treated as the criterion (Hsu et al., 2003). The PSCF values were
233 multiplied by a weighting function W_{ij} to reduce the effect of small values of n_{ij} and to
234 better reflect the uncertainty in the values for the cells with small n_{ij} values. The
235 weighting function W_{ij} is defined as follows (Polissar et al., 1999):

$$236 \quad W_{ij} = \begin{cases} 1.00, & 80 < n_{ij} \\ 0.70, & 20 < n_{ij} \leq 80 \\ 0.42, & 10 < n_{ij} \leq 20 \\ 0.05, & n_{ij} \leq 10 \end{cases}$$

237

238 The PSCF value can be interpreted as the conditional probability that ~~the~~-air
239 masses with pollutants concentration greater than the set criterion pass through the ij th

240 cell during transport to the receptor site (Wang et al., 2009). That is, cells with high
241 PSCF values are indicative of regions having high potential contributions to the
242 pollution at the receptor site.

243

244 3. Results and discussion

245 3.1 General characteristics of haze events

246 As illustrated in Fig. 2, the visibility varied from a few hundred meters to more than
247 50 km with a minimum value of only 322 m on Jan. 15, 2013, which was
248 accompanied by high RH (82%). During the 2-month observation period, there were a
249 ~~totally of~~ ten periods when visibility was below 10 km. ~~Excluding~~~~cept for~~ the five
250 periods ~~which were~~ accompanied by precipitation, the other five periods were
251 identified as haze events ~~were identified~~ and all of these events occurred in January
252 2013. During the haze occurrence, ~~the~~ hourly concentrations of PM_{2.5} often exceeded
253 150 µg m⁻³, with a maximum concentration of 324 µg m⁻³ observed on Jan. 14, 2013.
254 These concentrations were generally higher than those in normal periods. The daily
255 concentrations of PM_{2.5} on haze days varied from 148 to 196 µg m⁻³, which were 1.97
256 to 2.61 times the Grade II criteria of the national ambient air quality standard (75 µg
257 m⁻³). ~~These values is~~ ~~were~~ comparable to that observed~~the PM_{2.5} concentrations~~ in
258 Nanjing ~~where the with~~ average PM_{2.5} value of was 175.6 µg m⁻³, but ~~slightly~~~~little~~
259 higher than those in some other cities in YRD ~~where with the~~ mean values were
260 generally lower than 147.3 µg m⁻³ when haze occurred in Jan. 2013 (Wang et al.,
261 2014a; Wang et al., 2014d). The aerosol pollution happened in northeast China such
262 as in Beijing, Tianjin, and Shijiazhuang were much severer, for instance, the daily and
263 hourly concentrations of PM_{2.5} were up to 368 µg m⁻³ and 462 µg m⁻³ in Tianjin in
264 January 9 to 13, 2013, ~~and~~ the ~~hourly~~-maximum hourly values of approximately 1000
265 µg m⁻³ ~~was~~~~ere~~ recorded in Beijing and Shijiazhuang in Jan. 2013 (Ji et al., 2014; Han
266 et al., 2014; Wang et al., 2015).

267 ~~The duration of haze events comprised a~~ approximately 40% of the time in whole

268 January 2013 met haze weather criteria, whereas no haze appeared in December 2012.
269 LessLow amount of rainfall in ~~the~~ January might be one of the factors causing ~~the~~
270 long duration of haze. ~~The~~Relative humidity (RH) was reported to be an important
271 contributor to the visibility reduction. In ~~the~~ present study, ~~the RH increased with the~~
272 ~~reduction of~~visibility decreased with increasing RH, e.g. when RH increased from
273 42% to 78%, ~~the~~visibility decreased from 42 km at 2:00 p.m. on 17 January to 4 km
274 at 7:00 a.m. on 19 January. Statistically, ~~the~~RH was relatively higher during haze
275 occurrence than clear periods. Low wind speed, smaller than 5 m s⁻¹, ~~was~~
276 frequently observed during this winter. Furthermore, ~~the~~wind speeds ~~was~~ mostly
277 less than 1 m s⁻¹ during the haze events, lower than those in Beijing (Yang et al.,
278 2015). Besides, atmospheric pressure was also found to be relatively low during the
279 haze occurrences. The stagnant air, due to low wind speed and pressure, was
280 unfavorable for ~~the aerosol~~ horizontal transport or vertical diffusion ~~of aerosols~~, and
281 therefore resulted in~~leading to the increase of~~ aerosol accumulation~~concentration~~.
282 Therefore, unfavorable weather conditions (high RH, and low rainfall, wind speed and
283 atmospheric pressure) were among the causes ~~might provide external caused~~
284 beneficially for the ~~formation of~~ haze in January 2013 in Suzhou as well as
285 many other cities (Wang et al., 2014b; Wang et al., 2014c; Wang et al., 2014d; Han et
286 al., 2014; Yang et al., 2015).

287 In order to get more insights of the haze formation in this region, three haze
288 events, which occurred on Jan. 19, from Jan. 21 to 26, and on Jan. 30, respectively,
289 were further discussed below. Generally, the meteorological parameters and aerosol
290 pollution level were comparable during these three haze occurrences, except for the
291 relatively lower RH and higher temperature in the third haze events.–

292

293 **3.2 PM_{2.5} chemical composition and light extinction**

294 **3.2.1 PM_{2.5} chemical composition**

295 The temporal variations of the concentrations of water-soluble inorganic ions (WSIIs)
296 ~~we~~are illustrated in Fig. 3. The mean concentration of WSIs (including four anions
297 and five cations) was $48.8 \pm 24.6 \mu\text{g m}^{-3}$, accounting for 40% of $\text{PM}_{2.5}$ mass
298 concentration, ~~slightly little~~ lower than that in Beijing which was $69.4 \pm 55.8 \mu\text{g m}^{-3}$
299 and accounted for 43% of $\text{PM}_{2.5}$ (Tao et al., 2015). SO_4^{2-} was the most abundant
300 species in WSIs, with averaged value of $21.1 \pm 13.5 \mu\text{g m}^{-3}$, followed by NH_4^+ (13.9
301 $\pm 5.69 \mu\text{g m}^{-3}$) and NO_3^- ($10.7 \pm 6.75 \mu\text{g m}^{-3}$), accounting for 43%, 29% and 21% of
302 WSIs, respectively. These secondary inorganic components ~~in totally~~ constitute 93%
303 of total WSIs, close to the result in Beijing (Gao et al., 2015; Tao et al., 2015). The
304 rest of ions, Na^+ ($1.36 \pm 0.43 \mu\text{g m}^{-3}$), K^+ ($0.85 \pm 0.45 \mu\text{g m}^{-3}$), Cl^- ($0.54 \pm 1.28 \mu\text{g}$
305 m^{-3}), Ca^{2+} ($0.34 \pm 0.27 \mu\text{g m}^{-3}$), F^- ($0.06 \pm 0.72 \mu\text{g m}^{-3}$), Mg^{2+} ($0.05 \pm 0.07 \mu\text{g m}^{-3}$),
306 each had minor contribution ($< 3\%$) to WSIs.

307 NO_3^- and SO_4^{2-} are mainly formed from the transformation of their ~~respective~~
308 ~~gaseous~~ precursors of NO_x and SO_2 (Wang et al., 2005). The emission ratio of NO_x to
309 SO_2 was 17.2–52.6 for motor vehicles and 0.527–0.804 for stationary sources in the
310 Yangtze River Delta, which means that the emissions of SO_2 from motor vehicles
311 were much less than NO_x , but the emissions of SO_2 from stationary sources such as
312 power plants, industrial boilers and furnaces were relatively higher than NO_x (Fu et
313 al., 2008). Thus, the mass ratio of $\text{NO}_3^-/\text{SO}_4^{2-}$ could be used as an indicator of the
314 relative importance of mobile and stationary sources of sulfur and nitrogen in the
315 atmosphere (Arimoto et al., 1996). In ~~the~~ present study, the averaged ratios of
316 $\text{NO}_3^-/\text{SO}_4^{2-}$ and NO_x/SO_2 were 0.59 and 5.68, respectively, indicating that emissions
317 from vehicles and stationary sources were both important in Suzhou. The ratios of
318 $\text{NO}_3^-/\text{SO}_4^{2-}$ in this study ~~wasere~~ lower than ~~thatthe ratio~~ in Beijing, but higher than
319 those ~~reported~~ in Shanghai (0.43), Qingdao (0.35), Taiwan (0.20), and Guiyang (0.13)
320 (Wang et al., 2006; Yao et al., 2002; Hu et al., 2002a; Fang et al., 2002; Xiao and Liu,
321 2004).

322 The $\text{NO}_3^-/\text{SO}_4^{2-}$ ratio was relatively higher for 20% worst visibility ~~hours (0.58)~~
323 than 20% best visibility ~~hours (0.54), which were 0.58 and 0.54, respectively,~~

324 suggesting that vehicle emission might play an important role in haze pollution. This
325 was in agreement with the result in Guangzhou, where the $\text{NO}_3^-/\text{SO}_4^{2-}$ ratio was 1.02
326 under stagnation and 0.55 in normal days, but contrary to that in Beijing, where the
327 ratio in haze days (0.6489) was lower than in normal days (0.9683) (Tan et al., 2009;
328 Wang et al., 2006). In present study, NO_x concentration greatly exceeded that of SO_2
329 during haze period, coincided with the result in Guangzhou, but disagreed with that in
330 Beijing (Tan et al., 2009). Previous studies have indicated that high NO_x emission
331 may reduce the formation of OH and H_2O_2 , and further decrease the possibility of
332 SO_4^{2-} formation (Tan et al., 2009). Thus, the elevation of NO_3^- concentration under
333 worse visibility conditions was greater than that of SO_4^{2-} in both Suzhou and
334 Guangzhou. Besides of lower $\text{NO}_3^-/\text{SO}_4^{2-}$ ratio, Wang et al. also found lower NO_2/SO_2
335 ratio and lower ratio of ($\text{NO}_3^-/\text{SO}_4^{2-}$) to (NO_2/SO_2) in haze days than that in clear days
336 in Beijing, and summarized that the formation rate of nitrate might not be the
337 controlling factor for the nitrate concentrations in $\text{PM}_{2.5}$ (Wang et al., 2006). The low
338 $\text{NO}_3^-/\text{SO}_4^{2-}$ ratios found in haze days in Beijing was considered to be related to the
339 thermodynamic characteristic of NH_4NO_3 (Wang et al., 2006). The ratios of NO_x/SO_2
340 in present study were 6.89 for 20% worst visibility period higher than 4.30 for 20%
341 best visibility period. The ratios of ($\text{NO}_3^-/\text{SO}_4^{2-}$) to (NO_x/SO_2) were also lower for
342 worse visibility period in present study, in accordance with that in Beijing, suggesting
343 showing that the nitrate concentrations may be also greatly affected by the
344 re-volatilization of NH_4NO_3 (Tan et al., 2009) ~~as those in Beijing.~~

345 The carbonaceous species, constituting 22% of $\text{PM}_{2.5}$, were dominated by
346 organic carbons, which were $22.8 \pm 10.6 \mu\text{g m}^{-3}$ and 3 to 29 times of that of
347 elemental carbon ($2.79 \pm 2.58 \mu\text{g m}^{-3}$), similar to those in Beijing (Tao et al., 2015).
348 The relatively high ratios of OC/EC (10.6 ± 4.29), which were higher than the ratios
349 in Beijing (7.1 ± 0.5) and Jinan (7.15 ± 1.78), demonstrated the existence of
350 secondary organic carbon (SOC) (Ji et al., 2014; Zhang et al., 2014). The
351 concentrations of SOC were estimated by applying the EC tracer method, which has
352 been widely used to estimate the secondary organic aerosol contribution to $\text{PM}_{2.5}$

353 concentrations (Castro et al., 1999; Yang et al., 2005). The minimum ratio of OC/EC
354 was 3.09 in the present study. ~~So t~~The estimated ~~concentrations of~~ SOC ~~wasere~~ $14.2 \pm$
355 $5.69 \mu\text{g m}^{-3}$, contributing 65% on average to OC. The ~~ratios of~~ SOC/OC ~~wasere~~
356 higher than 0.5 during almost the whole sampling ~~periodtime~~ except ~~onfor the periods~~
357 ~~around~~ Jan. 30, when the third haze event occurred. This ratio was higher than most of
358 the results found in other areas such as in Beijing and Guangzhou (Yang et al., 2005;
359 Tan et al., 2009).

360 ~~Overall, according to the percentage of each species in PM_{2.5} mass, the m~~Major
361 components in PM_{2.5} were found to be SO₄²⁻ (17%), SOC (14%), NH₄⁺ (12%), NO₃⁻
362 (8%), and POC (6%) ~~with total percentage of 57%. It is noted that t~~The topfirst four
363 ~~componentspecies~~ were mainly from secondary sources. ~~In addition, the~~
364 ~~concentrations of~~ PM_{2.5} ~~wasere~~ significantly correlated with these secondary species,
365 revealing that gas to particle conversion ~~during winter in this region~~ was severe in
366 winter and had great impact on aerosol pollution in this region. It's worth noting that
367 the aerosol composition in the third haze event was distinct from the other two (Fig. 3)
368 as seen from the higher proportion of carbon species from primary emissions (POC
369 and EC) and lower fraction of secondary formation components (SIA and SOC),
370 indicating different haze formation mechanism in the third haze event.

371

372 **~~3.2.2 Variations of aerosol particles and precursors~~**

373 ~~Fig. 4 diagrammed the diurnal variation of meteorological parameters, various aerosol~~
374 ~~components and, the precursors and some other important gaseous species under three~~
375 ~~different visibility conditions (i.e., (1) all data, (2) visibility ≤ 10 km, (3) visibility $>$~~
376 ~~10 km). The daily variation of gas phase compounds were different between species~~
377 ~~and were mainly controlled by the direct surface emissions (such as NO_x, SO₂, and~~
378 ~~CO) or photochemical process (O₃). There were a distinct AM morning peak and a~~
379 ~~less distinct afternoon PM peak, consistent with morning and afternoon PM rush hours~~
380 ~~for NO_x and CO. This might related to the heavy traffic emission in the rush hours~~

381 and the strong elevation of the Planetary Boundary Layer heights at noon. In contrast,
382 there was only one mid-day peak for SO₂. This diurnal profiles were similar to those
383 observed in Guangzhou (Hu et al., 2002b) and Maryland (Antony Chen et al., 2001).
384 In the latter study, the dominant source of SO₂ was considered to be the long range
385 transport from the industrialized Midwest and with the deep boundary layer around
386 noon, SO₂ aloft mixed more effectively down to the surface and thus caused the
387 mid-day peak of SO₂. The reasons for the diurnal variation of SO₂ observed in present
388 study need further investigation. Similar to the diurnal distribution of SO₂, O₃ also
389 showed one distinct peak around noon due to the strong photochemistry at that time
390 (Quan et al., 2014).

391 For the aerosol components, EC which was also produced by the surface
392 emissions showed similar profile to NO_x and CO. Furthermore, EC had significantly
393 positive correlation with NO_x and CO, demonstrating that they had common sources,
394 mainly from vehicular exhaust. However, The diurnal profiles of the secondary
395 species were similar to their precursors but obviously affected by O₃
396 concentrations other factors such as solar radiation, which could promote the oxidation
397 of the precursors, as these species were mainly produced by chemical processes. For
398 instance, there was a 2-hour delay for sulfate to reach its peak compared to SO₂ due to
399 the transformation. This pattern was also observed in Guangzhou (Hu et al., 2002b).
400 NO₃⁻ and SOC exhibited similar diurnal variation as their precursors had common
401 sources and they both formed from secondary photochemical oxidation. The daily
402 profiles of NO₃⁻, NH₄⁺ and SOC showed lower concentrations around 15:00 (local
403 time) probably due to the high boundary layer and/or low concentration of precursors.
404 Besides, for NO₃⁻ and NH₄⁺, high temperature, which enhanced the evaporative loss,
405 and low relative humidity may also responsible for the low level.

406 Fig. 4 also suggested that both gas phase compounds and aerosol components all
407 showed similar pattern of diurnal variation but had different magnitudes of
408 concentrations for different visibility levels. These components except for O₃ all
409 showed relatively higher concentrations under low visibility especially for the

410 ~~secondary inorganic species, indicating the important impact of the formation of~~
 411 ~~secondary components on the visibility reduction. The relatively low levels of O₃~~
 412 ~~under low visible conditions might because of the decreased photochemical~~
 413 ~~production and the chemical conversions of SO₂ and NO_x to sulfate and nitrate. It is~~
 414 ~~worth noting that relatively high humidity which favored for the formation of sulfate~~
 415 ~~and nitrate was observed under low visibility conditions. In addition, it seemed that~~
 416 ~~low visibility was associated with southwest wind. This might related to the~~
 417 ~~topography. There are mountains located on the southwest which is not conducive to~~
 418 ~~the diffusion of pollutants.~~

419

420 **3.2.23 Light extinction coefficient**

421 In order to ~~appoint~~ determine the contribution of PM_{2.5} constituents to the visibility
 422 degradation, light extinction (b_{ext}) was reconstructed based on the revised IMPROVE
 423 algorithm. In the present study, the impact of fine soil and coarse mass were not
 424 included because of the lack of metal elements and coarse matter concentrations. ~~Thus,~~
 425 ~~the revised IMPROVE algorithm was modified as following:~~

$$\begin{aligned}
 426 \quad b_{ext} &= b_{s,p} + b_{a,p} + b_{a,g} + b_{s,g} \\
 427 \quad &\approx 2.2 \times f_s(RH) \times [\text{Small } (NH_4)_2SO_4] + 4.8 \times f_L(RH) \times [\text{Large } (NH_4)_2SO_4] \\
 428 \quad &+ 2.4 \times f_s(RH) \times [\text{Small } NH_4NO_3] + 5.1 \times f_L(RH) \times [\text{Large } NH_4NO_3] \\
 429 \quad &+ 2.8 \times [\text{Small OM}] + 6.1 \times [\text{Large OM}] \\
 430 \quad &+ 1.7 \times f_{ss}(RH) \times [\text{Sea Salt}] + 10 \times [\text{EC Mass}] + 0.33 \times [\text{NO}_2 \text{ (ppb)}] + \text{Rayleigh Scattering}
 \end{aligned}$$

431 The estimated b_{ext} ~~in present study wasere~~ $664 \pm 288 \text{ Mm}^{-1}$; and was significantly
 432 correlated with PM_{2.5} concentrations ($r = 0.94$, $p < 0.001$), demonstrating the strong
 433 influence of fine aerosols on visibility degradation.

434 The reconstructed light extinction coefficient was compared with that derived
 435 from visibility and that calculated using a regression model developed by Chen.
 436 Extinction coefficient is inversely correlated with visibility according to the

437 Koschmieder equation ($Vis = K/b_{ext}$) (Seinfeld and Pandis, 2012). By using a K value
438 of 3.912, a comparison of the light extinction coefficients derived from different
439 methods. he calculated b_{ext} . Visibility is inversely correlated with the extinction
440 coefficient according to the Koschmieder equation ($Vis = K/b_{ext}$). By using a K value
441 of 3.912, we further calculated the visibility based on the reconstructed b_{ext} . The
442 estimated visibilities were $7.47371 \pm 4.12234 \text{ Mm}^{-1}\text{-km}$, ranged from 2.57 km to
443 23.41 km. Although this was much lower than the measured visibility, which were
444 $15.0 \pm 8.50 \text{ km}$, coefficients obtained from IMPROVE algorithm. Nevertheless, the
445 estimated and measured visibility they had similar temporary trend and were
446 significantly correlated with each other ($r = 0.71, p < 0.001$). Another method applied
447 here to estimate b_{ext} was a 2-factor parameterization regression model based on RH
448 and aerosol volume concentration (Chen et al., 2012). The volume concentration can
449 be acquired from the mass concentration divided by an average particle density of 1.7
450 g cm^{-3} (Wehner et al., 2008). A comparison of b_{ext} reconstructed by IMPROVE
451 algorithm and the regression model is presented in Fig. 4. Generally, a strong
452 correlation was evident with a correlation coefficient higher than 0.97 ($R^2 = 0.952$),
453 confirming that the reconstructed b_{ext} from the IMPROVE algorithm was reliable. The
454 majority of b_{ext} was clustered near the 1:1 line for $b_{ext} < 500 \text{ Mm}^{-1}$, with the
455 corresponding RHs mainly below 75%. However, for $b_{ext} > 500 \text{ Mm}^{-1}$, the dispersion
456 of b_{ext} gradually increased, and most of the corresponding RH was higher than 75%.
457 There are two possibilities causing these deviations. The first one is the ignorance of
458 the impact of particle size distribution on light extinction in the 2-factor
459 parameterization model applied here, as the variation of aerosol mass or volume
460 fractions of different size particles can influence b_{ext} value especially under high RH
461 (Chen et al., 2012). The second one is from the uncertainties of in situ measurements
462 since RH sensor may have large errors under high RH condition. The regression
463 model result was directly controlled by the RH value, and the hygroscopic growth
464 factor in the IMPROVE algorithm depends on RH.

465

466 The light extinction ~~was~~ were mostly influenced by aerosol light scattering as the
 467 estimated $b_{s,p}$ ~~was~~ were $609 \pm 277 \text{ Mm}^{-1}$, accounting for 91% of ~~the~~ b_{ext} ~~(at least 75%)~~,
 468 while $b_{a,p}$ and the extinction coefficient by gaseous were only $27.9 \pm 25.8 \text{ Mm}^{-1}$ and
 469 $26.6 \pm 4.87 \text{ Mm}^{-1}$, respectively. The largest contributor to b_{ext} from the
 470 reconstructed chemical species in fine particles ~~to b_{ext}~~ was organic matter (OM),
 471 accounting for 40%, followed by $(\text{NH}_4)_2\text{SO}_4$, 34%, NH_4NO_3 , 16%, and EC , with their
 472 shares of 34%, 16% and 4%, respectively. Fractions of these ~~However, the percentage~~
 473 ~~contributors~~ varied greatly during over the study period, e.g. the contributions of
 474 NH_4NO_3 ranged from only 3% to up to 40%. Generally, the contributions of
 475 $(\text{NH}_4)_2\text{SO}_4$ and NH_4NO_3 were higher under low visibility period, increased from 30%
 476 and 11%, respectively, during the ~~under~~ 20% best visibility periods to 39% and 19%,
 477 respectively, during the ~~under~~ 20% worst visibility period, increased 1.3 and 1.7 times,
 478 respectively. While ~~Correspondingly~~, the contributions of OM and EC ~~were~~ reduced
 479 from 46% and 5%, respectively, under 20% best visibility period to 35% and 4%,
 480 respectively, during the same periods ~~under 20% worst visibility period~~. These results
 481 indicated the important role ~~of~~ sulfate and nitrate played on haze formation.

482 The percentages contribution to light extinction from individual ~~of the~~ aerosol
 483 components ~~contribute to the light extinction were~~ also varied with ~~experienced~~
 484 different variations in their fractions during different haze events and visibility
 485 conditions. ~~We compared~~ ~~the~~ percentage contributions of individual ~~these~~
 486 components during the best and worst ~~under~~ 20% best-visibility hours in each of the
 487 three haze events are compared and shown in Fig. 5 ~~conditions to those under 20%~~
 488 worst visibility conditions to investigate the controlling factor for the haze formation
 489 (Fig. 5). During the first haze event (on Jan. 19), the contributions of NH_4NO_3
 490 was ~~increased from only 8% under 20% best visibility to~~ and 24% during the ~~under~~
 491 20% best and worst visibility hours, respectively, while the corresponding numbers
 492 are ~~percentage of OM decreased from 48% and~~ to 37% for OM. ~~For~~ There were no
 493 significant differences between the two visibility categories for the contributions of
 494 $(\text{NH}_4)_2\text{SO}_4$ and EC , there was no significant change. During ~~For~~ the second haze

495 event (from Jan. 21 to 26), the fractions were 1.8, 1.5 and 1.3 times higher for
496 NH_4NO_3 , $(\text{NH}_4)_2\text{SO}_4$ and EC respectively but 1.2 times lower for OM under ~~worse~~
497 20% worst visibility condition than those under 20% best visibility condition during
498 this time. Overall, $(\text{NH}_4)_2\text{SO}_4$ made great contribution to the light extinction and
499 NH_4NO_3 had largest difference between 20% best and worst visibility conditions
500 during these two haze events. Therefore, secondary inorganic aerosols especially
501 NH_4NO_3 was likely the key component for the impaired visibility for these two haze
502 events. The elevated proportion of $(\text{NH}_4)_2\text{SO}_4$ and NH_4NO_3 during the heavy polluted
503 period was also observed in Beijing (Tao et al., 2015; Wang et al., 2015; Zheng et al.,
504 2015). A different trend of comparison between the best and worst visibility periods
505 was found in the third haze event (on Jan. 30) than in the first two. In the third event,
506 the percentage contributions of ~~Contrarily, during the third haze (on Jan. 30)~~
507 ~~increasing proportions of~~ OM and EC increased during the worst visibility period
508 compared to the best visibility period (from 40% to 49% and 6.8% to 11%,
509 respectively), while that of ~~accompanied with decreasing percentage of~~ $(\text{NH}_4)_2\text{SO}_4$
510 decreased (from 28% to 19%), ~~were found under worse visibility period, indicating~~
511 ~~that the e~~Carbonaceous components might be relatively played a more important role
512 for ~~the~~ visibility reduction in the third event. Therefore, there seems to be different
513 formation mechanisms for haze ~~eventsformation~~ in Suzhou.

514

515 3.3 Conversion from gas to particle phase

516 3.3.1 Variations of aerosol particles and precursors

517 Fig. 64 diagrammed the diurnal variations of meteorological parameters, various
518 aerosol components, the gaseous precursors, and some other important gaseous species
519 under three different visibility conditions: (i.e., (1) all data, (2) visibility ≤ 10 km, and
520 (3) visibility > 10 km). The daily variations of gas-phase compounds were different
521 between species and were mainly controlled by the direct surface emissions (such as
522 NO_x , SO_2 , and CO) or photochemical process (O_3). There were a distinct morning

523 peak and a less distinct afternoon peak, consistent with morning and afternoon rush
524 hours for NO_x and CO. This might be related to the heavy traffic emissions in the
525 rush hours and the strong elevation of the Planetary Boundary Layer heights at noon.
526 In contrast, there was only one mid-day peak for SO₂. This diurnal profiles were
527 similar to those observed in Guangzhou (Hu et al., 2002b) and Maryland (Antony
528 Chen et al., 2001). In the latter study, the dominant source of SO₂ was considered to
529 be the long range transport from the industrialized Midwest and with the deep
530 boundary layer around noon; SO₂ aloft mixed more effectively down to the surface
531 and thus caused the mid-day peak of SO₂. The reasons for the diurnal variation of SO₂
532 observed in the present study need further investigation. Similar to the diurnal
533 distribution of SO₂, O₃ also showed one distinct peak around noon due to the strong
534 photochemistry at that time (Quan et al., 2014).

535 For the aerosol components, EC which was also produced by the surface
536 emissions showed a profile similar-profile to NO_x and CO. Furthermore, EC had
537 significantly positive correlation with NO_x and CO, demonstrating that they had
538 common sources, mainly from vehicular exhaust. The diurnal profiles of the
539 secondary species were similar to their precursors but obviously affected by other
540 factors such as solar radiation, which could promote the oxidation of the precursors.
541 For instance, there was a 2-hour delay for sulfate to reach its peak compared to SO₂
542 due to the transformation processes. This pattern was also observed in Guangzhou
543 (Hu et al., 2002b). NO₃⁻ and SOC exhibited similar diurnal variation as their
544 precursors had common sources and they both formed from secondary photochemical
545 oxidation. The daily profiles of NO₃⁻, NH₄⁺ and SOC showed lower concentrations
546 around 15:00 (local time) probably due to the high boundary layer and/or low
547 concentration of precursors. Besides, for NO₃⁻ and NH₄⁺, high temperature, which
548 enhanced the evaporative loss, and low relative humidity may also be responsible for
549 the low levels.

550 Fig. 64 also suggested that both gas-phase compounds and aerosol components
551 all showed similar patterns of diurnal variations but had different magnitudes of

552 concentrations for different visibility levels. These components except for O₃ all
553 showed relatively higher concentrations under low visibility especially for the
554 secondary inorganic species, indicating the important impact of the formation of
555 secondary components on the visibility reduction. The relatively low levels of O₃
556 under low visible conditions might be due to ~~because of~~ the decreased photochemical
557 production and the chemical conversions of SO₂ and NO_x to sulfate and nitrate. It is
558 worth noting that the relatively high humidity which favored ~~for~~ the formation of
559 sulfate and nitrate was observed under low visibility conditions. In addition, it seemed
560 that low visibility was associated with southwest wind. This might related to the
561 topography. There are mountains located on the southwest which is not conducive to
562 the diffusion of pollutants.

563 In consideration of the distinct aerosol composition during the third haze, the
564 comparison of gaseous pollutants between the third and the first two haze episodes
565 were made. The concentrations of SO₂ and O₃ were comparable for these three haze
566 event. Contrarily, much higher levels of NO, CO and NO₂ were evident during the
567 third haze, in accordance with the high concentrations of POC and EC. These species
568 (NO, CO, NO₂, POC and EC) ~~were~~ had good correlations with each other.
569 Furthermore, they had similar diurnal variations and exhibited extremely high levels
570 in the morning rush hours on January 30 when the third haze occurred. These results
571 implied that there were common sources for these species, mainly from vehicle
572 exhaust emission. —

574 **3.3.2 Formation mechanisms of sulfate and nitrate**

575 As discussed earlier, the chemical formation of sulfate and nitrate from SO₂ and NO₂
576 respectively, should play important roles for visibility reduction, especially for the
577 first two haze events. The sulfur oxidation ratio, defined as $SOR = n\text{-SO}_4^{2-} / (n\text{-SO}_4^{2-} +$
578 $n\text{-SO}_2)$ and the nitrogen oxidation ratio, defined as $NOR = n\text{-NO}_3^- / (n\text{-NO}_3^- + n\text{-NO}_2)$
579 were used as indicators of the secondary transformation processes. The daily

580 variations of NOR showed similar patterns as those of NH_4^+ and NO_3^- . Likewise,
581 SOR had similar diurnal changes as SO_4^{2-} . The values of SOR and NOR increased
582 more than 1.3 and 2.0 times, respectively, during the first two haze periods compared
583 to clear periods. Both SOR and NOR were higher with lower visibility (Fig. 6),
584 implying greater oxidation of gaseous species and more elevated secondary aerosols.
585 This was supported by the evidently higher concentrations of SO_4^{2-} , NH_4^+ , and NO_3^-
586 under worse visibility conditions in the first two haze events. Almost no elevating
587 levels of SOR, NOR or SIA were observed in the third haze, again confirming that the
588 SIA formation may not be the predominant factor controlling the occurrence of this
589 haze event.

590 The formation of SO_4^{2-} from SO_2 was mainly ascribed to the gas-phase oxidation
591 withby OH and H_2O_2 radical or heterogeneous oxidation (Wang et al., 2006; Zhao et
592 al., 2013). The gas-phase reaction is a strong function of temperature and
593 heterogeneous reactions always associated with high RH (Sun et al., 2006; Sun et al.,
594 2014; Sun et al., 2013a). However, weak correlations were found between SOR and
595 either temperature ($r = 0.174$, $p < 0.01$) or RH ($r = 0.150$, $p < 0.01$) in the present
596 study, indicating the complex formation mechanism of sulfate.

597 Many studies suggested that sulfate from aqueous SO_2 oxidation catalyzed by
598 transition metals was more significant during winter haze rather than gas-phase
599 oxidation (Li et al., 2011; Sun et al., 2013b; Zhao et al., 2013). Our measurement also
600 found that the heterogeneous oxidation was an important sulfate formation pathway in
601 this study area. As shown in Fig. 7, high concentrations of NO_2 accompanied with
602 ultralow level of O_3 less than 10 ppb and low amount of solar radiation were observed
603 during most of the time in the haze period, such as from 12 PM to 10 AM on 19
604 January and from 21 to 34 January. These results revealed the rather weak
605 photochemical activities during these time windows. The high levels of NO_2 and
606 weak photochemical activities could result in insufficient production of oxidants (OH
607 and H_2O_2 radicals) for gas-phase oxidation (Hua et al., 2008). Thus, other oxidation
608 reactions other than gas-phase oxidation likely explained the formation of abundant

609 secondary sulfates during the haze episode. The high RH (> 70%) during these haze
610 period was a beneficial factor for aqueous-phase oxidation of SO₂ to sulfate. Besides,
611 the calculation results using the Extended AIM Aerosol Thermodynamic Model
612 (E-AIM, Model II) (Clegg et al., 1998) (<http://www.aim.env.uea.ac.uk/aim/aim.php>)
613 showed a significant increase of the liquid water content when RH > 70%. These
614 results highlight the importance of aqueous-phase reaction to the secondary
615 transformation of SO₂.

616 The concentrations of O₃ were not extremely low during the whole haze period,
617 such as during daytime on January 23 and 25; the O₃ levels were as usual and had
618 obvious diurnal variations with one distinct peak around noon. RH was lower than
619 70% and sulfate was primarily in the solid phase at these times, indicating that
620 gas-phase oxidation was probably the dominant pathway for sulfate formation.
621 Aqueous-phase oxidation likely became predominant at night. This could explain the
622 high SOR in the afternoon and the sustained high level at night.

623 ~~The daily variation of NOR showed similar pattern as NH₄⁺ and NO₃⁻; likewise,~~
624 ~~SOR had similar diurnal change as SO₄²⁻, indicating the influence from NO_x or SO₂~~
625 ~~and O₃. Additionally, it is interesting to notice that under low visibility conditions~~
626 ~~during nighttime when O₃ concentrations were extremely low, there was still a rapid~~
627 ~~chemical conversion from gaseous to particle phase especially for sulfate particles.~~
628 ~~This conversion might mainly be produced through the processes other than the~~
629 ~~photochemical activities such as heterogeneous reactions in the aqueous surface layer~~
630 ~~of pre-existing particles or in cloud processes. The higher humidity during that time~~
631 ~~and the significant positive correlations between SOR and humidity through the~~
632 ~~whole study period again seem to validate that the heterogeneous process likely~~
633 ~~dominate the sulfate formation. This was consistent with the finding by Hewitt that~~
634 ~~liquid phase chemical conversion process was responsible for the formation of sulfate~~
635 ~~partieles in winter (Hewitt, 2001).~~

636 ~~Compared to the formation of sulfate, the contributions of various conversion~~
637 ~~pathways to nitrate formation were less known (Pathak et al., 2009). In this section,~~

638 ~~we examined in detail the possible causes of nitrate in PM_{2.5}.~~ Nitrate formation is
639 mainly through gas-phase oxidation of NO₂ by OH during daylight and the
640 heterogeneous reactions of nitrate radical during nighttime (Seinfeld and Pandis,
641 2012). ~~Figure-Fig. 7-8~~ showed the nitrate-to-sulfate molar ratio ($[\text{NO}_3^-]/[\text{SO}_4^{2-}]$) as a
642 function of the ammonium-to-sulfate molar ratio ($[\text{NH}_4^+]/[\text{SO}_4^{2-}]$), which can provide
643 an insight into the formation pathway of the secondary species (Jansen et al., 2014;
644 Pathak et al., 2009; He et al., 2012).

645 The relative abundance of nitrate linearly increased with the increasing
646 ammonium-to-sulfate molar ratio. Fitting a linear regression line resulted in an
647 intercept of $[\text{NH}_4^+]/[\text{SO}_4^{2-}]$ -axis of 1.51, indicating that nitrate formation via
648 homogeneous reaction of HNO₃ with NH₃ became significant at $[\text{NH}_4^+]/[\text{SO}_4^{2-}] >$
649 1.51 (Pathak et al., 2009; Jansen et al., 2014; He et al., 2012) ~~(Pathak et al., 2004;~~
650 ~~Pathak and Chan, 2005)~~. Pathak et al. (2009) also reported an intercept value of 1.5
651 for ~~a variety of several~~ cities worldwide while Jansen et al. (2014) found a ~~little~~
652 ~~slightly~~ smaller intercept value of 1.38 for Hangzhou. The ammonium concentration
653 in excess of the amount at which nitrate formation became evident was defined as
654 excess ammonium ($[\text{NH}_4^+]_{\text{exc}} = ([\text{NH}_4^+]/[\text{SO}_4^{2-}] - 1.51) \times [\text{SO}_4^{2-}]$). The concentrations of
655 excess ammonium were always higher than 0 and linearly correlated with nitrate
656 concentration, as shown in ~~Fig. ure~~ 8. This indicated that the formation of nitrate was
657 strongly associated with ammonium formation. In other words, when the excess
658 ammonium was > 0 , the gas-phase homogeneous reaction between the ambient
659 ammonia and nitric acid was responsible for forming nitrate (Pathak et al., 2009;
660 Jansen et al., 2014). The slope of 0.37 for the regression and the scattering of the data
661 indicated that the excess ammonium was bound to species other than nitrate, such as
662 chloride, bisulfate, etc. The significance of gas-phase homogeneous reaction to nitrate
663 formation has been reported for many cities (Jansen et al., 2014; Pathak et al., 2009).
664 However, as mentioned above, in some cases during haze period, the conditions
665 (ultralow ozone concentrations, low solar radiation and high NO₂) were not favorable
666 for the gas-phase oxidation. Relatively high RH were often observed in those cases,

667 which may have favored the gas to particle partitioning of nitrate acid and ammonia
668 (Sun et al., 2011). Furthermore, the E-AIM calculation results manifested that the
669 nitrate partly or completely existed in the aqueous phase during those conditions.
670 Therefore, we assumed that heterogeneous chemistry, such as heterogeneous
671 hydrolysis of N₂O₅ (N₂O₅ + H₂O (aq) → 2HNO₃) or equilibrium partitioning (HNO₃
672 (g) + NH₃ (g) ↔ NH₄⁺ (aq) + NO₃⁻ (aq)) also contributed to the formation of nitrate
673 under high RH conditions. This was supported by the fact that in Fig. 8 more plots
674 were deviated from the regression line when RH were relatively high. The importance
675 of Besides, a model study also verified that aqueous-phase oxidation of NO_x was of
676 minor importance for nitrate production in the atmosphere (Pandis and Seinfeld,
677 1989). But contrarily, heterogeneous reactions for nitrate formation were considered
678 to be significantly important in the production of both sulfate and nitrate also reported
679 in other studies (Sun et al., 2011; Zheng et al., 2015) ~~(Sun et al., 2011).~~

680

681 **3.4 Regional sources deduced from trajectory and PSCF analyses**

682 The regional sources and transport of air pollutants exert a profound impact on local
683 air quality in YRD region as it is located in the typical monsoon region (Ding et al.,
684 2013). Therefore, trajectory clustering method was employed to examine the pathway
685 of air masses and to look into the chemical compositions and light extinction
686 coefficients among the air masses with different origination. The calculated 48-h
687 back trajectories were clustered into six clusters (Fig. 9 and Table 1), i.e. six air mass
688 transport pathways. As can be seen, Table 1 summarized the percentage of trajectories
689 for each trajectory cluster and the corresponding mean concentrations of PM_{2.5} and
690 major aerosol species. air masses reaching at Suzhou mainly came from local areas,
691 the nearby provinces (cluster 2, accounting 31.7%), and the northwestern areas
692 (cluster 1 and 3, both accounted for 20.6%).

693 High aerosol concentrations were associated with these trajectories. This was
694 reasonable considering that these air masses passed over some highly industrialized

695 cities, such as Hefei, Nanjing, and Hangzhou (Fig. 1). ~~The trajectory clusters were~~
696 ~~dominated by cluster 2, accounting for 31.7%, followed by cluster 1 and 3, both~~
697 ~~accounted for 20.6%, and the rest clusters, cluster 4, 5 and 6 accounted for 12.7%,~~
698 ~~6.3% and 7.9%, respectively. Obviously, air masses mainly originated from the north~~
699 ~~and southwest (cluster 1 to 4).~~

700 The mean concentrations of PM_{2.5} and main aerosol species varied with certain
701 types of air masses. The highest mean concentration of PM_{2.5} (167 $\mu\text{g m}^{-3}$) was
702 associated with C3 cluster with the air masses originating from northwest and passed
703 over Anhui and Jiangsu provinces. The air from the C1, C2 and C4 areas were also
704 related to relatively high PM_{2.5} concentrations, which were 129 $\mu\text{g m}^{-3}$, 117 $\mu\text{g m}^{-3}$
705 and 103 $\mu\text{g m}^{-3}$ respectively. These air masses all passed over some highly
706 industrialized cities, such as Qingdao, Nanjing, and Hangzhou (Fig. 1). Relatively low
707 concentrations levels of PM_{2.5} were associated with related to clusters C5 (84 $\mu\text{g m}^{-3}$)
708 and C6 (87 $\mu\text{g m}^{-3}$). The trajectories of C5 and C6 mostly originated from southeast
709 ~~and northeast respectively.~~ Based on the pathways and origins, these air masses were
710 expected to bring in relatively clean air from the East China Sea and the Yellow Sea
711 and consequently reduced the aerosol pollution in Suzhou.

712 Aerosols had high fractions of secondary inorganic ions (39%-42%) and
713 relatively low contributions of OC (15%-16%) when the air masses fell in the C1, C3
714 and C4, while had relatively high percentage of OC (36%) when the air masses fell
715 into the C5. These differences of aerosol concentrations and composition in different
716 clusters may result in distinct light extinction coefficients and species contributions to
717 visibility reduction when air masses originated from different directions (Fig. 9).
718 Similar to PM_{2.5}, the reconstructed b_{ext} was the highest when air masses originated
719 from the Northwest area (C3) and was relatively low when air masses fell into C5 and
720 C6 areas. However, the lowest value of b_{ext} was in the C6 instead of C5 for the lowest
721 PM_{2.5} level, because of the higher contribution of OM in the C5. For the major
722 components in PM_{2.5}, the highest averaged concentrations were associated with C3
723 cluster for sulfate, nitrate and ammonium but with C5 cluster for both OC and EC.

724 Accordingly, the composition profiles of these major species were different between
725 clusters. C1, C2, C3 and C4 trajectory clusters had similar composition with relatively
726 higher fractions of secondary inorganic ions (secondary inorganic ions > 35%, OC <
727 19%) compared to C5 and C6 clusters which both had relatively high contribution of
728 OC (secondary inorganic ions < 30%, OC > 23%).

729 These differences of PM_{2.5} concentrations and compositions in different clusters
730 may result in distinct light extinction coefficients and species contributions to
731 visibility reduction when air mass originated from different directions (Fig. 9).
732 Similar to PM_{2.5}, b_{ext} values were higher when the air masses originated from the
733 Northwest area (C3), whereas b_{ext} were relatively low when air masses fell into C5
734 and C6 areas. AS and OM were the dominant species determining the light
735 extinction for all clusters. However, differently, AS was the predominant contributor
736 to light extinction for trajectories from north and northwest (C1, C3, C4), while in
737 other cases the light extinction was primarily affected by OM. AN was the third
738 highest contributor in all trajectory clusters with the largest contribution when air
739 masses originated from northwest.

740 The origins of air masses in different haze events were further analyzed to
741 interpret the relative contributions of chemical species to visibility reduction that
742 differed between haze events. Most air masses fell into C1 and C3 (air masses from
743 north and northwest, respectively) in the first two haze occurrence while all air mass
744 trajectories were in C2 (air masses from south local and nearby areas) for the third
745 haze event. The contribution of OM to the total light extinction was higher in the third
746 haze event than in the first two as discussed early, consistent with the results for
747 cluster analysis that the light extinction was primarily impacted by AS for C1 and C3
748 but by OM for C2. These results manifested that the third haze event was mainly
749 contributed by the primary emission of carbon species from the local and/or
750 surrounding areas.

751 the air mass originated from southwest and passed over Zhejiang province might
752 play a key role in the high contribution of OM in the third haze event.

753 It should be noted that air mass back trajectory analysis only suggests the
754 originations and pathways of air masses but does not directly reveal the exact sources.
755 Based on the results of trajectory analysis, the PSCF method was applied to explore
756 the likely regional sources of major components in PM_{2.5}, including sulfate, nitrate,
757 OC, and EC, as illustrated in Fig. 10. Generally, PM_{2.5} and the five aerosol species in
758 Suzhou were mainly affected by local sources and nearby cities. Specifically, the
759 higher value for PM_{2.5} and the aerosol components were all localized in northwest to
760 the south, covering surrounding cities in Jiangsu and near the border of Anhui and
761 Zhejiang provinces. Additionally, these species were all affected by pollutions from
762 Anhui province. Sulfate, nitrate and ammonium had similar spatial distributions, and
763 relatively more affected by the north and northwest cities in Shandong, Jiangsu and
764 Anhui provinces while pollutions from south cities in Zhejiang province had more
765 impact on OC and EC in studied area than sulfate, nitrate and ammonium.

767 4. Conclusions

768 Heavy aerosol pollution occurred in Suzhou in January 2013 with daily PM_{2.5}
769 concentrations on haze days 1.97 to 2.61 times higher than Grade II criteria of the
770 national ambient air quality standard (75 $\mu\text{g m}^{-3}$) and maximum value of 324 $\mu\text{g m}^{-3}$
771 on Jan. 14, 2013. Unfavorable weather conditions (high RH, low rainfall, wind speed
772 and atmospheric pressure) especially high RH together with increased air pollutants
773 produced from local and nearby sources were responsible~~might provide beneficial~~
774 ~~conditions~~ for these haze formation.

775 ~~During the first two haze periods, WSH and carbonaceous species both increased~~
776 ~~during the haze events and~~ the major aerosol components ~~situations~~ were SO₄²⁻, NO₃⁻,
777 NH₄⁺, and SOC, which were mainly from secondary sources. Furthermore, SOR and
778 NOR both increased under worst visibility conditions, revealing efficient~~severe~~ gas to
779 particle conversion ~~during winter in this region~~. Additionally, The conversion
780 mechanisms were further analyzed for sulfate and nitrate. Rapid chemical conversion
781 from gas to particle phase for sulfate particles under extremely low O₃ concentrations

782 ~~and significant correlations between SOR and humidity demonstrated that~~
783 ~~heterogeneous process might dominate the sulfate formation. However, the result of~~
784 ~~($[\text{NO}_3^-]/[\text{SO}_4^{2-}]$) as a function of ($[\text{NH}_4^+]/[\text{SO}_4^{2-}]$) showed that the formation of~~
785 ~~ammonium nitrate via the homogeneous gas-phase reaction was favored.~~

786 ~~The reconstructed light extinction coefficients based on the revised IMPROVE~~
787 ~~algorithm were $664 \pm 288 \text{ Mm}^{-1}$, and mainly contributed by OM (40%), $(\text{NH}_4)_2\text{SO}_4$~~
788 ~~(34%), NH_4NO_3 (16%), and EC (4%). The contributions of these species experienced~~
789 ~~different variations in their fractions under different visibility conditions. Generally,~~
790 ~~the contributions share of $(\text{NH}_4)_2\text{SO}_4$ and NH_4NO_3 to the reconstructed b_{ext} based on~~
791 ~~IMPROVE were higher under low visibility conditions while those the percentages of~~
792 ~~OM and EC were higher increased under high visibility conditions, indicating that~~
793 ~~secondary inorganic aerosols especially NH_4NO_3 seemed to be very important for the~~
794 ~~impaired visibility. Gas-phase homogeneous reaction might dominate the formation of~~
795 ~~sulfate and nitrate under low RH conditions while heterogeneous process might be~~
796 ~~responsible when RH were relatively high.~~

797 ~~But d~~Distinctively, ~~high proportion of carbon species from primary emission and~~
798 ~~lower fraction of secondary formation components were observed in the third haze.~~
799 ~~The SOR and NOR during the third haze episode were comparable to clean days.~~
800 ~~Moreover,~~ increasing proportions of OM and EC accompanied with decreasing
801 percentage of $(\text{NH}_4)_2\text{SO}_4$ were found under worst visibility conditions when the third
802 haze occurred. ~~These results, suggested suggesting that the carbon components from~~
803 ~~the primary emission might be relatively important for the visibility reduction for this~~
804 haze event.

805 ~~These differences in different haze events might be greatly affected by the~~
806 ~~pathways of air masses according to trajectory clustering analysis.~~

807 ~~The result of t~~Trajectory clustering analysis showed that the air quality in Suzhou
808 was mostly affected by air masses originating from North and Southwestern areas
809 which were associated with high aerosol concentrations. Distinct aerosol composition
810 profiles, light extinction coefficients and species contributions to visibility reduction

811 were observed when air masses originated from different directions, e.g. AS was the
812 predominant contributor to light extinction for trajectories from north and northwest,
813 while in other cases the light extinction was primarily affected by OM.

814 The likely sources of aerosol and the major species based on the PSCF method
815 were mainly from local anthropogenic activities and source emissions transported
816 from nearby cities. The northwestern to southern regions may be important sources of
817 aerosols and the major components. The northern and northwestern areas were
818 predominant source regions for sulfate, nitrate and ammonium aerosols, whereas the
819 southern area could be the common source region for carbonaceous species. This
820 information has the implications for the importance of collaborative air pollution
821 control strategy in the Yangtze River Delta Region.

822

823 **Acknowledgements**

824 This work was supported by the National Natural Science Foundation of China
825 projects (41403089, 41375123), the "Strategic Priority Research Program" of the
826 Chinese Academy of Sciences (KJZD-EW-TZ-G06-04), and the State Environmental
827 Protection Key Laboratory of Sources and Control of Air Pollution Complex
828 (SCAPC201310).

829

830 **References**

- 831 Antony Chen, L. W., Doddridge, B. G., Dickerson, R. R., Chow, J. C., Mueller, P. K.,
832 Quinn, J., and Butler, W. A.: Seasonal variations in elemental carbon aerosol,
833 carbon monoxide and sulfur dioxide: Implications for sources, *Geophys. Res. Lett.*,
834 28, 1711-1714, doi: 10.1029/2000gl012354, 2001.
- 835 Arimoto, R., Duce, R. A., Savoie, D. L., Prospero, J. M., Talbot, R., Cullen, J. D.,
836 Tomza, U., Lewis, N. F., and Jay, B. J.: Relationships among aerosol constituents
837 from Asia and the North Pacific during PEM-West A, *J. Geophys. Res.-Atmos.*,
838 101, 2011-2023, doi: 10.1029/95jd01071, 1996.
- 839 Ashbaugh, L. L., Malm, W. C., and Sadeh, W. Z.: A residence time probability
840 analysis of sulfur concentrations at Grand-Canyon-National-Park, *Atmos. Environ.*,
841 19, 1263-1270, doi: 10.1016/0004-6981(85)90256-2, 1985.
- 842 Bae, M.-S., Schauer, J. J., DeMinter, J. T., Turner, J. R., Smith, D., and Cary, R. A.:
843 Validation of a semi-continuous instrument for elemental carbon and organic
844 carbon using a thermal-optical method, *Atmos. Environ.*, 38, 2885-2893, doi:
845 10.1016/j.atmosenv.2004.02.027, 2004.
- 846 Castro, L. M., Pio, C. A., Harrison, R. M., and Smith, D. J. T.: Carbonaceous aerosol
847 in urban and rural European atmospheres: estimation of secondary organic carbon
848 concentrations, *Atmos. Environ.*, 33, 2771-2781, doi:
849 10.1016/S1352-2310(98)00331-8, 1999.
- 850 Charlson, R. J., Lovelock, J. E., Andreae, M. O., and Warren, S. G.: Oceanic
851 phytoplankton, atmospheric sulfur, cloud albedo and climate, *Nature*, 326, 655-661,
852 doi: 10.1038/326655a0, 1987.
- 853 Chen, J., Zhao, C. S., Ma, N., Liu, P. F., Göbel, T., Hallbauer, E., Deng, Z. Z., Ran, L.,
854 Xu, W. Y., Liang, Z., Liu, H. J., Yan, P., Zhou, X. J., and Wiedensohler, A.: A
855 parameterization of low visibilities for hazy days in the North China Plain, *Atmos.*
856 *Chem. Phys.*, 12, 4935-4950, doi: 10.5194/acp-12-4935-2012, 2012.
- 857 Chen, R., Zhao, Z., and Kan, H.: Heavy smog and hospital visits in Beijing, China,
858 *Am. J. Respir. Crit. Care Med.*, 188, 1170-1171, doi:

859 10.1164/rccm.201304-0678LE, 2013.

860 Chow, J. C., Doraiswamy, P., Watson, J. G., Antony-Chen, L. W., Ho, S. S. H., and
861 Sodeman, D. A.: Advances in integrated and continuous measurements for particle
862 mass and chemical, composition, *J. Air Waste Manage. Assoc.*, 58, 141-163, doi:
863 10.3155/1047-3289.58.2.141, 2008.

864 Clegg, S. L., Brimblecombe, P., and Wexler, A. S.: Thermodynamic model of the
865 system $\text{H}^+ - \text{NH}_4^+ - \text{SO}_4^{2-} - \text{NO}_3^- - \text{H}_2\text{O}$ at tropospheric temperatures, *The Journal of*
866 *Physical Chemistry A*, 102, 2137-2154, doi: 10.1021/jp973042r, 1998.

867 Ding, A. J., Fu, C. B., Yang, X. Q., Sun, J. N., Zheng, L. F., Xie, Y. N., Herrmann, E.,
868 Nie, W., Petaja, T., Kerminen, V. M., and Kulmala, M.: Ozone and fine particle in
869 the western Yangtze River Delta: an overview of 1 yr data at the SORPES station,
870 *Atmos. Chem. Phys.*, 13, 5813-5830, doi: 10.5194/acp-13-5813-2013, 2013.

871 Fang, G. C., Chang, C. N., Wu, Y. S., Fu, P. P. C., Yang, C. J., Chen, C. D., and Chang,
872 S. C.: Ambient suspended particulate matters and related chemical species study in
873 central Taiwan, Taichung during 1998-2001, *Atmos. Environ.*, 36, 1921-1928, doi:
874 10.1016/S1352-2310(02)00187-5, 2002.

875 Fu, Q., Zhuang, G., Wang, J., Xu, C., Huang, K., Li, J., Hou, B., Lu, T., and Streets, D.
876 G.: Mechanism of formation of the heaviest pollution episode ever recorded in the
877 Yangtze River Delta, China, *Atmos. Environ.*, 42, 2023-2036, doi:
878 10.1016/j.atmosenv.2007.12.002, 2008.

879 Gao, J., Tian, H., Cheng, K., Lu, L., Zheng, M., Wang, S., Hao, J., Wang, K., Hua, S.,
880 Zhu, C., and Wang, Y.: The variation of chemical characteristics of $\text{PM}_{2.5}$ and PM_{10}
881 and formation causes during two haze pollution events in urban Beijing, China,
882 *Atmos. Environ.*, 107, 1-8, doi: 10.1016/j.atmosenv.2015.02.022, 2015.

883 Han, S., Wu, J., Zhang, Y., Cai, Z., Feng, Y., Yao, Q., Li, X., Liu, Y., and Zhang, M.:
884 Characteristics and formation mechanism of a winter haze-fog episode in Tianjin,
885 China, *Atmos. Environ.*, 98, 323-330, doi: 10.1016/j.atmosenv.2014.08.078, 2014.

886 He, K., Zhao, Q., Ma, Y., Duan, F., Yang, F., Shi, Z., and Chen, G.: Spatial and
887 seasonal variability of $\text{PM}_{2.5}$ acidity at two Chinese megacities: insights into the
888 formation of secondary inorganic aerosols, *Atmos. Chem. Phys.*, 12, 1377-1395,

889 doi: 10.5194/acp-12-1377-2012, 2012.

890 Hewitt, C. N.: The atmospheric chemistry of sulphur and nitrogen in power station
891 plumes, *Atmos. Environ.*, 35, 1155-1170, doi: 10.1016/S1352-2310(00)00463-5,
892 2001.

893 Hsu, Y. K., Holsen, T. M., and Hopke, P. K.: Comparison of hybrid receptor models to
894 locate PCB sources in Chicago, *Atmos. Environ.*, 37, 545-562, doi:
895 10.1016/S1352-2310(02)00886-5, 2003.

896 Hu, M., He, L. Y., Zhang, Y. H., Wang, M., Kim, Y. P., and Moon, K. C.: Seasonal
897 variation of ionic species in fine particles at Qingdao, China, *Atmos. Environ.*, 36,
898 5853-5859, doi: 10.1016/S1352-2310(02)00581-2, 2002a.

899 Hu, M., Zhou, F., Shao, K., Zhang, Y., Tang, X., and Slanina, J.: Diurnal variations of
900 aerosol chemical compositions and related gaseous pollutants in Beijing and
901 Guangzhou, *J. Environ. Sci. Health A Tox. Hazard. Subst. Environ. Eng.*, 37,
902 479-488, doi: 10.1081/ese-120003229, 2002b.

903 Hua, W., Chen, Z. M., Jie, C. Y., Kondo, Y., Hofzumahaus, A., Takegawa, N., Chang,
904 C. C., Lu, K. D., Miyazaki, Y., Kita, K., Wang, H. L., Zhang, Y. H., and Hu, M.:
905 Atmospheric hydrogen peroxide and organic hydroperoxides during
906 PRIDE-PRD'06, China: their concentration, formation mechanism and contribution
907 to secondary aerosols, *Atmos. Chem. Phys.*, 8, 6755-6773, doi:
908 10.5194/acp-8-6755-2008, 2008.

909 Huang, R. J., Zhang, Y., Bozzetti, C., Ho, K. F., Cao, J. J., Han, Y., Daellenbach, K. R.,
910 Slowik, J. G., Platt, S. M., Canonaco, F., Zotter, P., Wolf, R., Pieber, S. M., Bruns,
911 E. A., Crippa, M., Ciarelli, G., Piazzalunga, A., Schwikowski, M., Abbaszade, G.,
912 Schnelle-Kreis, J., Zimmermann, R., An, Z., Szidat, S., Baltensperger, U., El
913 Haddad, I., and Prevot, A. S.: High secondary aerosol contribution to particulate
914 pollution during haze events in China, *Nature*, 514, 218-222, doi:
915 10.1038/nature13774, 2014.

916 Jansen, R. C., Shi, Y., Chen, J., Hu, Y., Xu, C., Hong, S., Li, J., and Zhang, M.: Using
917 hourly measurements to explore the role of secondary inorganic aerosol in PM_{2.5}
918 during haze and fog in Hangzhou, China, *Adv. Atmos. Sci.*, 31, 1427-1434, doi:

919 10.1007/s00376-014-4042-2, 2014.

920 Ji, D., Li, L., Wang, Y., Zhang, J., Cheng, M., Sun, Y., Liu, Z., Wang, L., Tang, G., Hu,
921 B., Chao, N., Wen, T., and Miao, H.: The heaviest particulate air-pollution episodes
922 occurred in northern China in January, 2013: Insights gained from observation,
923 *Atmos. Environ.*, 92, 546-556, doi: 10.1016/j.atmosenv.2014.04.048, 2014.

924 Khoder, M. I.: Atmospheric conversion of sulfur dioxide to particulate sulfate and
925 nitrogen dioxide to particulate nitrate and gaseous nitric acid in an urban area,
926 *Chemosphere*, 49, 675-684, doi: 10.1016/S0045-6535(02)00391-0, 2002.

927 Li, W., Zhou, S., Wang, X., Xu, Z., Yuan, C., Yu, Y., Zhang, Q., and Wang, W.:
928 Integrated evaluation of aerosols from regional brown hazes over northern China in
929 winter: Concentrations, sources, transformation, and mixing states, *J Geophys Res*,
930 116, doi: 10.1029/2010jd015099, 2011.

931 Pathak, R. K., Wu, W. S., and Wang, T.: Summertime PM_{2.5} ionic species in four
932 major cities of China: nitrate formation in an ammonia-deficient atmosphere,
933 *Atmos. Chem. Phys.*, 9, 1711-1722, doi: 10.5194/acp-9-1711-2009, 2009.

934 Pathak, R. K., Wang, T., and Wu, W. S.: Nighttime enhancement of PM_{2.5} nitrate in
935 ammonia-poor atmospheric conditions in Beijing and Shanghai: Plausible
936 contributions of heterogeneous hydrolysis of N₂O₅ and HNO₃ partitioning, *Atmos.*
937 *Environ.*, 45, 1183-1191, doi: 10.1016/j.atmosenv.2010.09.003, 2011.

938 Pitchford, M., Maim, W., Schichtel, B., Kumar, N., Lowenthal, D., and Hand, J.:
939 Revised algorithm for estimating light extinction from IMPROVE particle
940 speciation data, *J. Air Waste Manage. Assoc.*, 57, 1326-1336, doi:
941 10.3155/1047-3289.57.11.1326, 2007.

942 Polissar, A. V., Hopke, P. K., Paatero, P., Kaufmann, Y. J., Hall, D. K., Bodhaine, B.
943 A., Dutton, E. G., and Harris, J. M.: The aerosol at Barrow, Alaska: long-term
944 trends and source locations, *Atmos. Environ.*, 33, 2441-2458, doi:
945 10.1016/S1352-2310(98)00423-3, 1999.

946 Quan, J., Tie, X., Zhang, Q., Liu, Q., Li, X., Gao, Y., and Zhao, D.: Characteristics of
947 heavy aerosol pollution during the 2012–2013 winter in Beijing, China, *Atmos.*
948 *Environ.*, 88, 83-89, doi: 10.1016/j.atmosenv.2014.01.058, 2014.

949 Ramanathan, V., and Vogelmann, A. M.: Greenhouse effect, atmospheric solar
950 absorption and the Earth's radiation budget: From the Arrhenius-Langley era to the
951 1990s, *Ambio*, 26, 38-46, 1997.

952 Seinfeld, J. H., and Pandis, S. N.: *Atmospheric Chemistry and Physics: From Air*
953 *Pollution to Climate Change*, Second ed., John Wiley & Sons, Hoboken, New
954 Jersey, 2012.

955 Sun, Y., Zhuang, G., Tang, A., Wang, Y., and An, Z.: Chemical Characteristics of
956 PM_{2.5} and PM₁₀ in Haze–Fog Episodes in Beijing, *Environ. Sci. Technol.*, 40,
957 3148-3155, doi: 10.1021/es051533g, 2006.

958 Sun, Y., Jiang, Q., Wang, Z., Fu, P., Li, J., Yang, T., and Yin, Y.: Investigation of the
959 sources and evolution processes of severe haze pollution in Beijing in January
960 2013, *J. Geophys. Res.: Atmos.*, 119, 4380-4398, doi: 10.1002/2014jd021641,
961 2014.

962 Sun, Y. L., Zhang, Q., Schwab, J. J., Chen, W. N., Bae, M. S., Lin, Y. C., Hung, H. M.,
963 and Demerjian, K. L.: A case study of aerosol processing and evolution in summer
964 in New York City, *Atmos. Chem. Phys.*, 11, 12737-12750, doi:
965 10.5194/acp-11-12737-2011, 2011.

966 Sun, Y. L., Wang, Z. F., Fu, P. Q., Jiang, Q., Yang, T., Li, J., and Ge, X. L.: The impact
967 of relative humidity on aerosol composition and evolution processes during
968 wintertime in Beijing, China, *Atmos. Environ.*, 77, 927-934, doi:
969 10.1016/j.atmosenv.2013.06.019, 2013a.

970 Sun, Y. L., Wang, Z. F., Fu, P. Q., Yang, T., Jiang, Q., Dong, H. B., Li, J., and Jia, J. J.:
971 Aerosol composition, sources and processes during wintertime in Beijing, China,
972 *Atmos. Chem. Phys.*, 13, 4577-4592, doi: 10.5194/acp-13-4577-2013, 2013b.

973 Tan, J., Duan, J., He, K., Ma, Y., Duan, F., Chen, Y., and Fu, J.: Chemical
974 characteristics of PM_{2.5} during a typical haze episode in Guangzhou, *J. Environ.*
975 *Sci.*, 21, 774-781, doi: 10.1016/s1001-0742(08)62340-2, 2009.

976 Tao, J., Zhang, L. M., Ho, K. F., Zhang, R. J., Lin, Z. J., Zhang, Z. S., Lin, M., Cao, J.
977 J., Liu, S. X., and Wang, G. H.: Impact of PM_{2.5} chemical compositions on aerosol
978 light scattering in Guangzhou - the largest megacity in South China, *Atmos. Res.*,

979 135, 48-58, doi: 10.1016/j.atmosres.2013.08.015, 2014.

980 Tao, J., Zhang, L., Gao, J., Wang, H., Chai, F., and Wang, S.: Aerosol chemical
981 composition and light scattering during a winter season in Beijing, *Atmos. Environ.*,
982 110, 36-44, doi: 10.1016/j.atmosenv.2015.03.037, 2015.

983 Tegen, I., Koch, D., Lacis, A. A., and Sato, M.: Trends in tropospheric aerosol loads
984 and corresponding impact on direct radiative forcing between 1950 and 1990: A
985 model study, *J. Geophys. Res.-Atmos.*, 105, 26971-26989, doi:
986 10.1029/2000jd900280, 2000.

987 Tie, X., Madronich, S., Li, G., Ying, Z., Weinheimer, A., Apel, E., and Campos, T.:
988 Simulation of Mexico City plumes during the MIRAGE-Mex field campaign using
989 the WRF-Chem model, *Atmos. Chem. Phys.*, 9, 4621-4638, doi:
990 10.5194/acp-9-4621-2009, 2009a.

991 Tie, X., Wu, D., and Brasseur, G.: Lung cancer mortality and exposure to atmospheric
992 aerosol particles in Guangzhou, China, *Atmos. Environ.*, 43, 2375-2377, doi:
993 10.1016/j.atmosenv.2009.01.036, 2009b.

994 Trebs, I., Meixner, F. X., Slanina, J., Otjes, R., Jongejan, P., and Andreae, M. O.:
995 Real-time measurements of ammonia, acidic trace gases and water-soluble
996 inorganic aerosol species at a rural site in the Amazon Basin, *Atmos. Chem. Phys.*,
997 4, 967-987, doi: 10.5194/acp-4-967-2004, 2004.

998 Wang, H., An, J., Shen, L., Zhu, B., Pan, C., Liu, Z., Liu, X., Duan, Q., Liu, X., and
999 Wang, Y.: Mechanism for the formation and microphysical characteristics of
1000 submicron aerosol during heavy haze pollution episode in the Yangtze River Delta,
1001 China, *Sci. Total Environ.*, 490, 501-508, doi: 10.1016/j.scitotenv.2014.05.009,
1002 2014a.

1003 Wang, H., Xu, J., Zhang, M., Yang, Y., Shen, X., Wang, Y., Chen, D., and Guo, J.: A
1004 study of the meteorological causes of a prolonged and severe haze episode in
1005 January 2013 over central-eastern China, *Atmos. Environ.*, 98, 146-157, doi:
1006 10.1016/j.atmosenv.2014.08.053, 2014b.

1007 Wang, J., Wang, S., Jiang, J., Ding, A., Zheng, M., Zhao, B., Wong, D. C., Zhou, W.,
1008 Zheng, G., Wang, L., Pleim, J. E., and Hao, J.: Impact of aerosol-meteorology

1009 interactions on fine particle pollution during China's severe haze episode in
1010 January 2013, *Environ. Res. Lett.*, *9*, doi: 10.1088/1748-9326/9/9/094002, 2014c.

1011 Wang, Y., Zhuang, G. S., Tang, A. H., Yuan, H., Sun, Y. L., Chen, S. A., and Zheng, A.
1012 H.: The ion chemistry and the source of PM_{2.5} aerosol in Beijing, *Atmos. Environ.*,
1013 *39*, 3771-3784, doi: 10.1016/j.atmosenv.2005.03.013, 2005.

1014 Wang, Y., Zhuang, G., Sun, Y., and An, Z.: The variation of characteristics and
1015 formation mechanisms of aerosols in dust, haze, and clear days in Beijing, *Atmos.*
1016 *Environ.*, *40*, 6579-6591, doi: 10.1016/j.atmosenv.2006.05.066, 2006.

1017 Wang, Y., Yao, L., Wang, L., Liu, Z., Ji, D., Tang, G., Zhang, J., Sun, Y., Hu, B., and
1018 Xin, J.: Mechanism for the formation of the January 2013 heavy haze pollution
1019 episode over central and eastern China, *Sci. China-Earth Sci.*, *57*, 14-25, doi:
1020 10.1007/s11430-013-4773-4, 2014d.

1021 Wang, Y. H., Liu, Z. R., Zhang, J. K., Hu, B., Ji, D. S., Yu, Y. C., and Wang, Y. S.:
1022 Aerosol physicochemical properties and implications for visibility during an
1023 intense haze episode during winter in Beijing, *Atmos. Chem. Phys.*, *15*, 3205-3215,
1024 doi: 10.5194/acp-15-3205-2015, 2015.

1025 Wang, Y. Q., Zhang, X. Y., and Draxler, R. R.: TrajStat: GIS-based software that uses
1026 various trajectory statistical analysis methods to identify potential sources from
1027 long-term air pollution measurement data, *Environ. Modell. Softw.*, *24*, 938-939,
1028 doi: 10.1016/j.envsoft.2009.01.004, 2009.

1029 Warneck, P.: *Chemistry of the natural atmosphere*, Academic press, 1999.

1030 Wehner, B., Birmili, W., Ditas, F., Wu, Z., Hu, M., Liu, X., Mao, J., Sugimoto, N., and
1031 Wiedensohler, A.: Relationships between submicrometer particulate air pollution
1032 and air mass history in Beijing, China, 2004-2006, *Atmos. Chem. Phys.*, *8*,
1033 6155-6168, doi: 10.5194/acp-8-6155-2008, 2008.

1034 Xiao, H. Y., and Liu, C. Q.: Chemical characteristics of water-soluble components in
1035 TSP over Guiyang, SW China, 2003, *Atmos. Environ.*, *38*, 6297-6306, doi:
1036 10.1016/j.atmosenv.2004.08.033, 2004.

1037 Yang, F. M., He, K. B., Ma, Y. L., Zhang, Q., Cadle, S. H., Chan, T., and Mulawa, P.
1038 A.: Characterization of carbonaceous species of ambient PM_{2.5} in Beijing, China, *J.*

1039 Air Waste Manage. Assoc., 55, 984-992, doi: 10.1080/10473289.2005.10464699,
1040 2005.

1041 Yang, Y., Liu, X., Qu, Y., Wang, J., An, J., Zhang, Y., and Zhang, F.: Formation
1042 mechanism of continuous extreme haze episodes in the megacity Beijing, China, in
1043 January 2013, *Atmos. Res.*, 155, 192-203, doi: 10.1016/j.atmosres.2014.11.023,
1044 2015.

1045 Yao, X. H., Chan, C. K., Fang, M., Cadle, S., Chan, T., Mulawa, P., He, K. B., and Ye,
1046 B. M.: The water-soluble ionic composition of PM_{2.5} in Shanghai and Beijing,
1047 China, *Atmos. Environ.*, 36, 4223-4234, doi: 10.1016/S1352-2310(02)00342-4,
1048 2002.

1049 Yu, H. B., Liu, S. C., and Dickinson, R. E.: Radiative effects of aerosols on the
1050 evolution of the atmospheric boundary layer, *J. Geophys. Res.-Atmos.*, 107, AAC
1051 3-1–AAC 3-14, doi: 10.1029/2001jd000754, 2002.

1052 Yu, S., Zhang, Q., Yan, R., Wang, S., Li, P., Chen, B., Liu, W., and Zhang, X.: Origin
1053 of air pollution during a weekly heavy haze episode in Hangzhou, China, *Environ.*
1054 *Chem. Lett.*, 12, 543-550, doi: 10.1007/s10311-014-0483-1, 2014.

1055 Zhang, J., Chen, J., Yang, L., Sui, X., Yao, L., Zheng, L., Wen, L., Xu, C., and Wang,
1056 W.: Indoor PM_{2.5} and its chemical composition during a heavy haze-fog episode at
1057 Jinan, China, *Atmos. Environ.*, 99, 641-649, doi: 10.1016/j.atmosenv.2014.10.026,
1058 2014.

1059 Zhang, Q., Quan, J., Tie, X., Li, X., Liu, Q., Gao, Y., and Zhao, D.: Effects of
1060 meteorology and secondary particle formation on visibility during heavy haze
1061 events in Beijing, China, *Sci. Total Environ.*, 502, 578-584, doi:
1062 10.1016/j.scitotenv.2014.09.079, 2015.

1063 Zhang, X. Y., Wang, Y. Q., Niu, T., Zhang, X. C., Gong, S. L., Zhang, Y. M., and Sun,
1064 J. Y.: Atmospheric aerosol compositions in China: spatial/temporal variability,
1065 chemical signature, regional haze distribution and comparisons with global
1066 aerosols, *Atmos. Chem. Phys.*, 12, 779-799, doi: 10.5194/acp-12-779-2012, 2012.

1067 Zhao, X. J., Zhao, P. S., Xu, J., Meng, W., Pu, W. W., Dong, F., He, D., and Shi, Q. F.:
1068 Analysis of a winter regional haze event and its formation mechanism in the North

1069 China Plain, *Atmos. Chem. Phys.*, 13, 5685-5696, doi: 10.5194/acp-13-5685-2013,
1070 2013.

1071 Zheng, G. J., Duan, F. K., Su, H., Ma, Y. L., Cheng, Y., Zheng, B., Zhang, Q., Huang,
1072 T., Kimoto, T., Chang, D., Poeschl, U., Cheng, Y. F., and He, K. B.: Exploring the
1073 severe winter haze in Beijing: the impact of synoptic weather, regional transport
1074 and heterogeneous reactions, *Atmos. Chem. Phys.*, 15, 2969-2983, doi:
1075 10.5194/acp-15-2969-2015, 2015.

1076

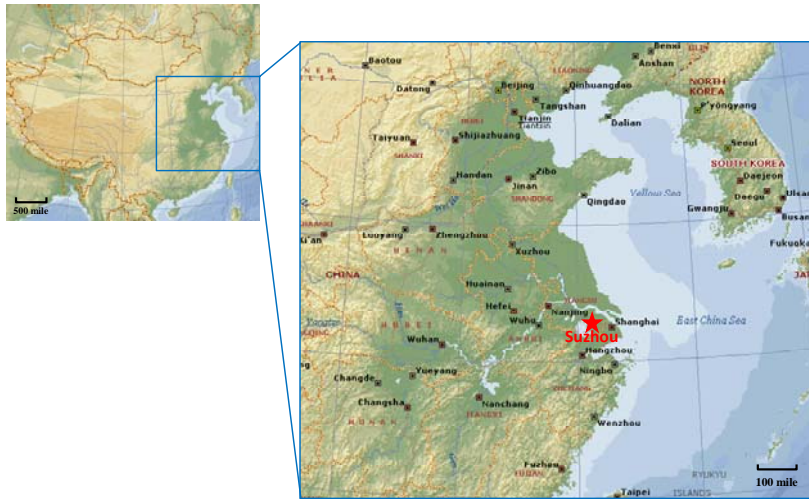
1077

1078 Table 1. The percentages of air masses from each trajectory cluster and associated~~the~~
 1079 mean b_{ext} (Mm^{-1}) and mean concentrations ($\mu\text{g m}^{-3}$) of $\text{PM}_{2.5}$ and its major chemical
 1080 components, and mean b_{ext} (Mm^{-1})~~selected aerosol species in the identified trajectory~~
 1081 clusters.

	1	2	3	4	5	6
Percent (%)	20.6	31.7	20.6	12.7	6.3	7.9
$\text{PM}_{2.5}$	129	117	167	103	84.0	87.4
OC	21.1	22.8	25.3	16.4	30.5	20.3
EC	2.05	3.87	2.21	1.45	3.90	1.86
Sulfate	22.9	18.2	32.4	23.1	8.85	8.39
Nitrate	11.5	10.0	16.9	7.84	3.26	7.91
Ammonium	15.2	12.3	18.9	12.4	7.93	9.88
b_{ext}	675	597	921	556	548	463

1082

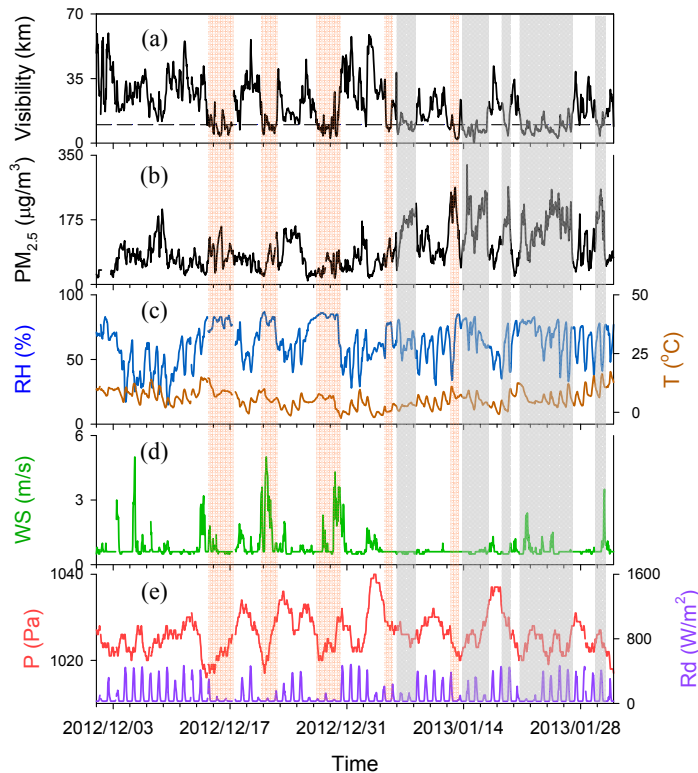
1083



1084

1085 Figure 1. The sampling site in Suzhou. The locations of ~~some~~ major cities with a
 1086 population of more than 1 million (such as Qingdao, Nanjing and Hangzhou) are
 1087 marked with a square symbol. The topographical map was derived from Microsoft®
 1088 Encarta® 2009 © 1993 - 2008.

1089

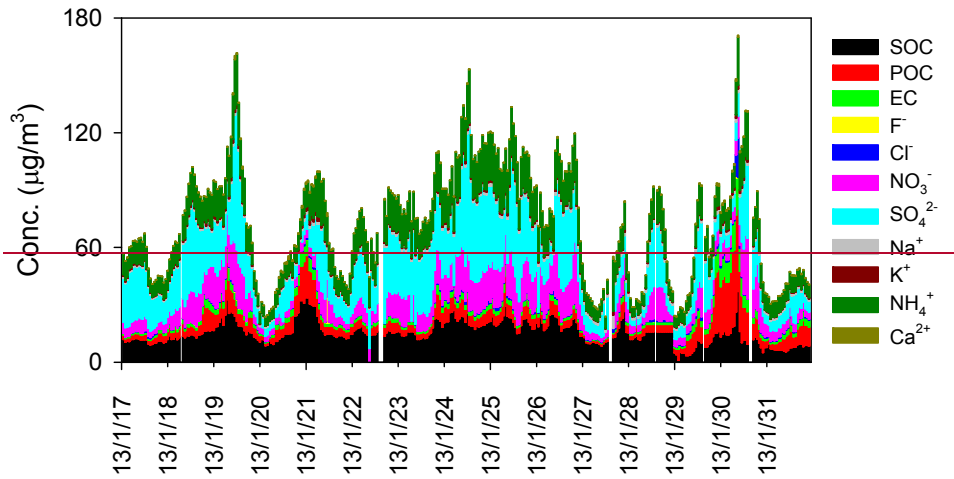


1090

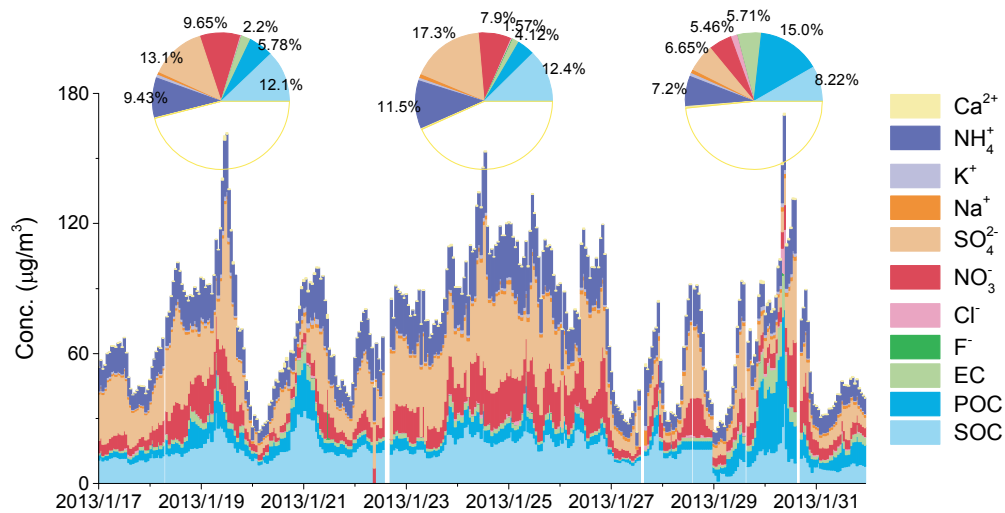
1091 Figure 2. Time series of (a) visibility; (b) $PM_{2.5}$ concentration; (c) relative humidity
 1092 (RH) and temperature (T); (d) wind speed (WS) and pressure (P); and (e) solar
 1093 radiation (Rd). The shaded areas in orange represent periods when visibility were

1094 lower than 10 km and accompanied by precipitation. The shaded areas in grey
 1095 represent haze periods.

1096



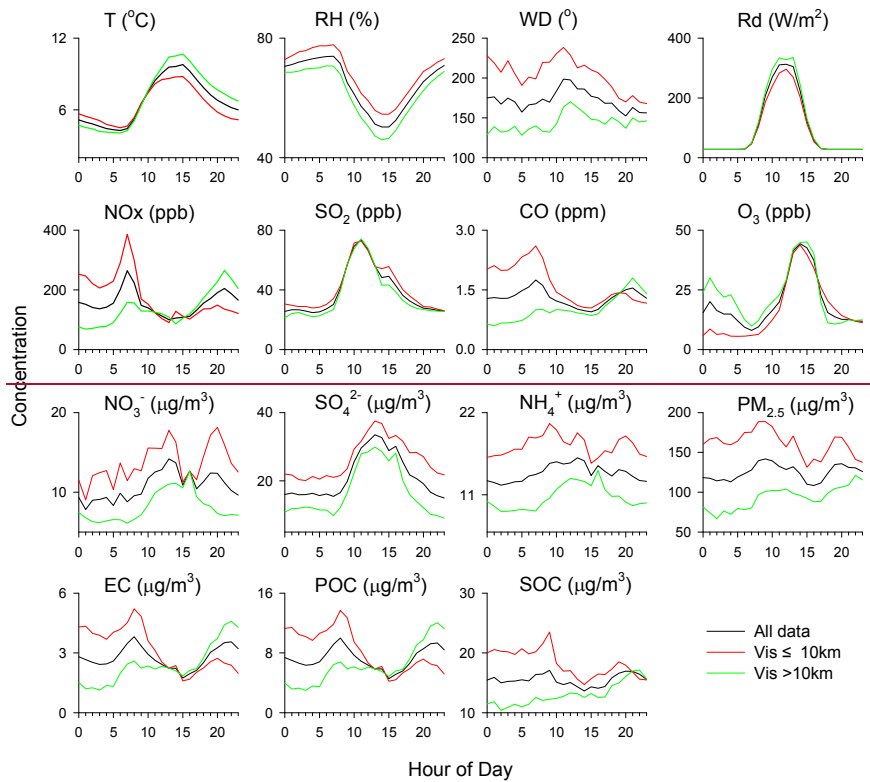
1097



1098

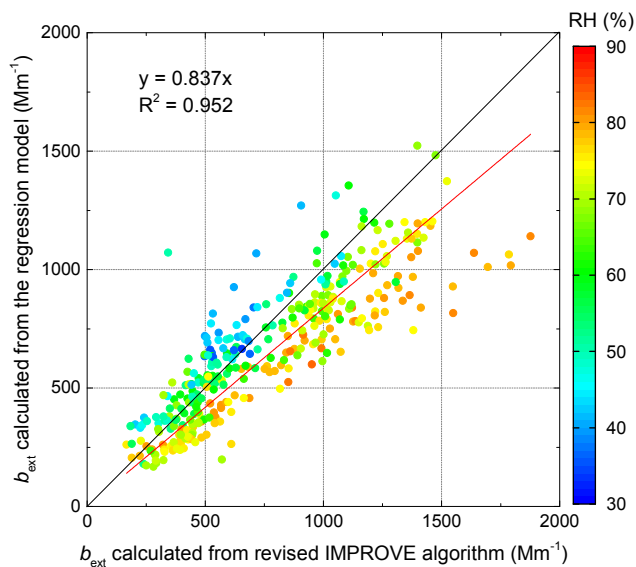
1099 Figure 3. Temporal distribution of water soluble inorganic ions and carbonaceous
 1100 species. The aerosol composition in the three haze events was also illustrated in the
 1101 pie chart.

1102



1103

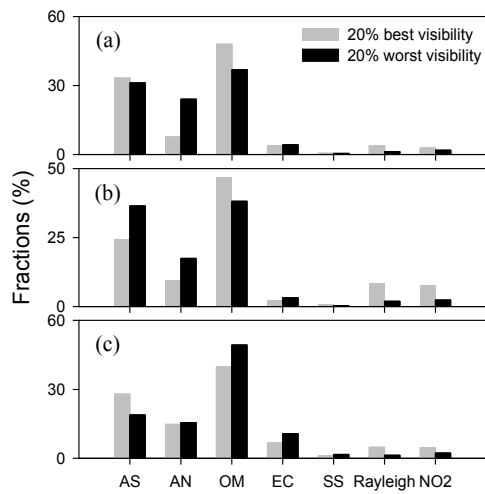
1104 Figure 4. Diurnal profiles of meteorological variables, aerosol precursors (NO_x , SO_2),
 1105 CO , O_3), $\text{PM}_{2.5}$, and major aerosol compounds (NO_3^- , SO_4^{2-} , NH_4^+ , EC , POC , SOC)
 1106 under different visibility conditions.



1107

1108 Figure 4. Comparison of the calculated b_{ext} between those obtained from the
 1109 regression equation and those from the IMPROVE algorithm.

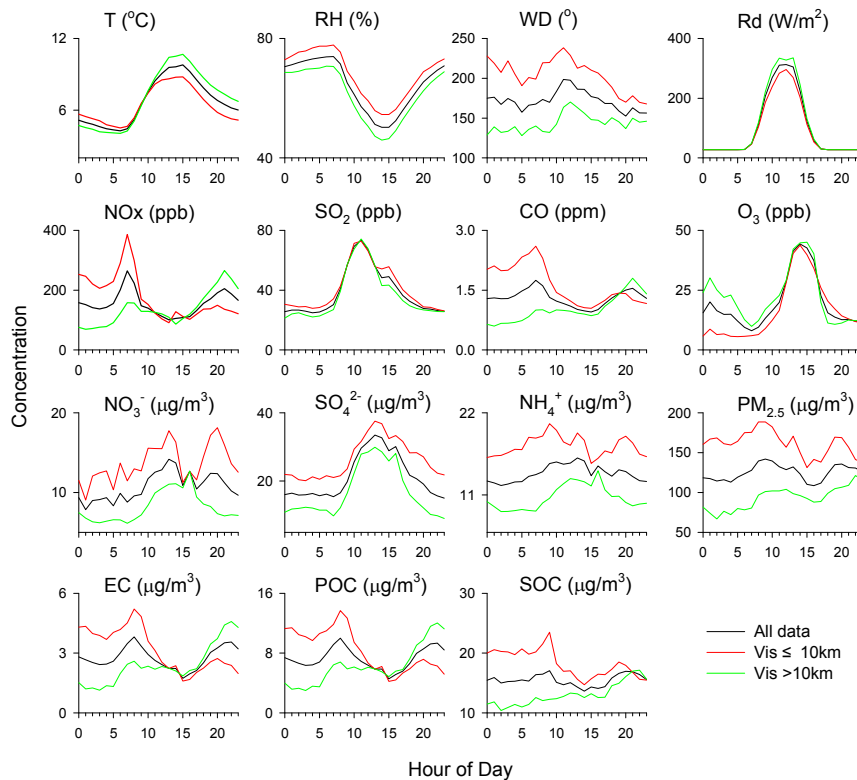
1110



1111

1112 Figure 5. Relative contributions of various chemical components in PM_{2.5}
 1113 (ammonium sulfate (AS), ammonium nitrate (AN), OM, and EC) to the total light
 1114 extinction under 20% best and 20% worst visibility conditions during the first (a),
 1115 second (b), and third (c) haze events.

1116

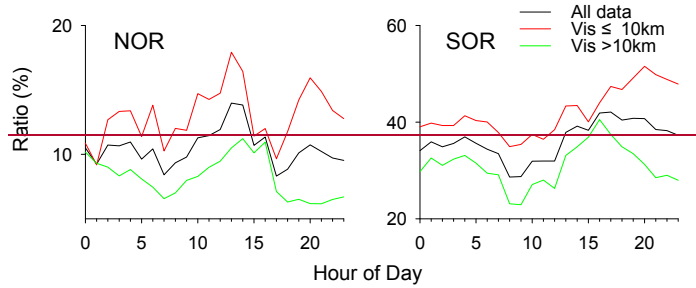


1117

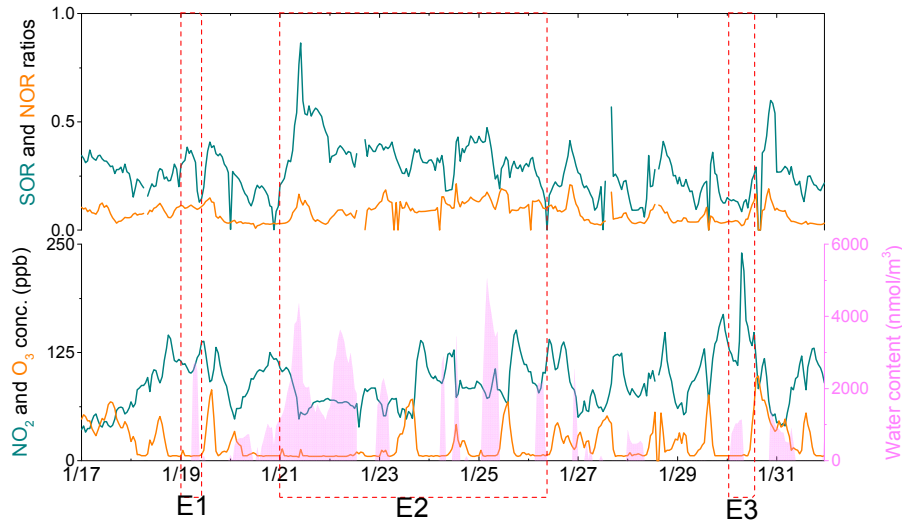
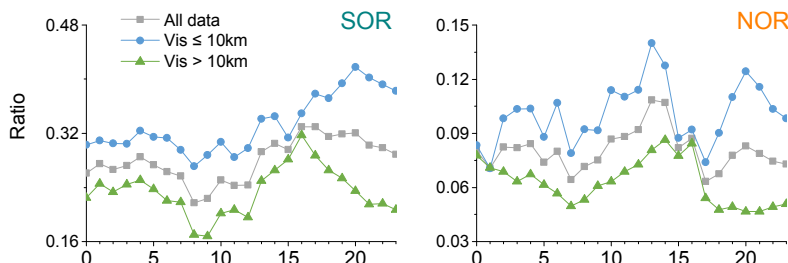
1118 Figure 6. Diurnal profiles of meteorological variables, aerosol precursors (NO_x, SO₂),

1119 CO, O₃, PM_{2.5}, and major aerosol compounds (NO₃⁻, SO₄²⁻, NH₄⁺, EC, POC, SOC)
 1120 under different visibility conditions.

1121



1122

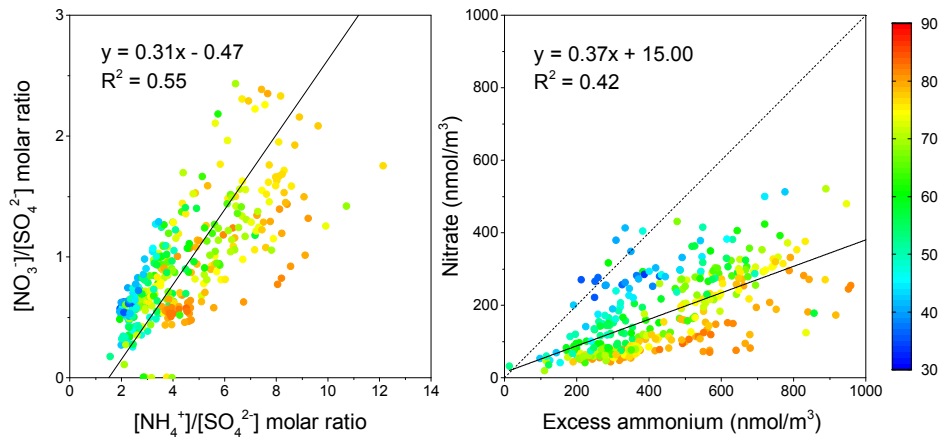


1123

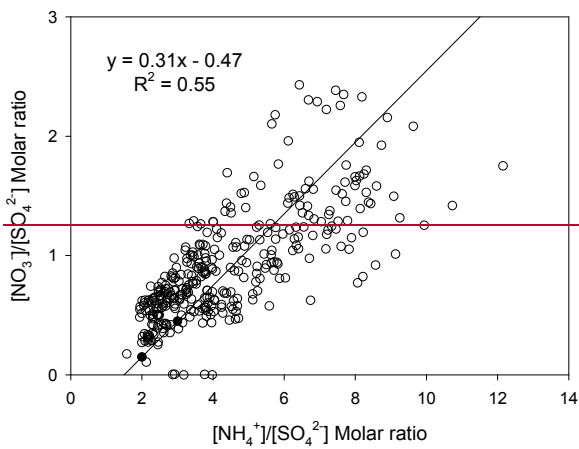
1124 Figure 76. Temporary distributions of SOR, NOR, NO₂, O₃ and aerosol water content.

1125 Diurnal profiles of NOR and SOR ratios under different visibility conditions.

1126



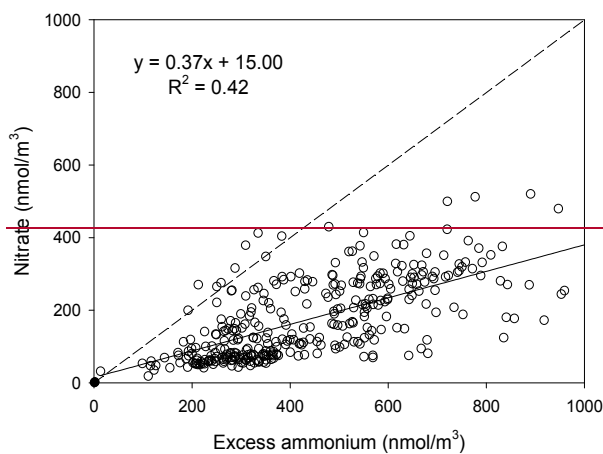
1127



1128

1129 Figure 78. Nitrate to sulfate molar ratio as a function of ammonium to sulfate molar
 1130 ratio- (left) and relationship

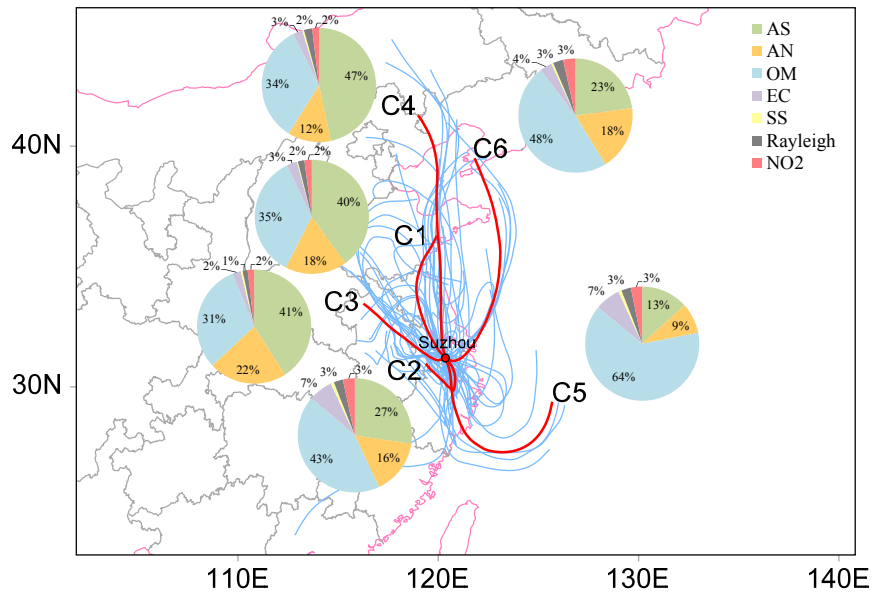
1131



1132

1133 Figure 8. Relationship between molar concentrations of nitrate and excess ammonium
 1134 (right).

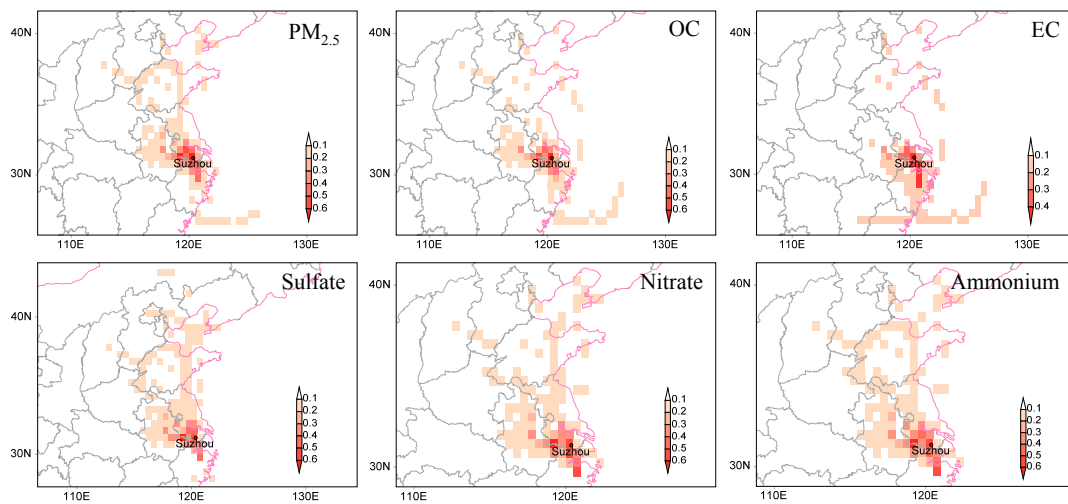
1135



1136

1137 Figure 9. Backward air mass trajectories and six mean trajectories after the cluster
 1138 analysis at the sampling site during Jan. 17 to 31. Relative contributions of various
 1139 chemical components to the total light extinction in different clusters are illustrated.

1140



1141

1142 Figure 10. The PSCF maps for PM_{2.5}, OC, EC, sulfate, nitrate, and ammonium.

1143